HGT

Evaluation of the Toxicity and Efficacy of an Adeno-Associated Viral Vector Expressing *BEST1* Delivered by Subretinal Injection in a Canine Model of Human Bestrophinopathy

Alexa Gray,[1,†] Jennifer C. Kwok,[1,†] Yu Sato,[1] Charles-Antoine Assenmacher,[2] Mayur Choudhary,[3] Ash Jayagopal,[3] Peiying Hua,[4] Gui-Shuang Ying,[4] Malgorzata Swider,[4] Alexander Sumaroka,[4] Artur V. Cideciyan,[4] Aguirre D. Gustavo,[1] and William A. Beltran[1,*]

[1]*Division of Experimental Retinal Therapies, Department of Clinical Sciences & Advanced Medicine, School of Veterinary Medicine, University of Pennsylvania, Philadelphia, Pennsylvania, USA;* [2]*Comparative Pathology Core, Department of Pathobiology, School of Veterinary Medicine, University of Pennsylvania, Philadelphia, Pennsylvania, USA;* [3]*Opus Genetics, Inc., Durham, North Carolina, USA; and* [4]*Center for Hereditary Retinal Degenerations, Department of Ophthalmology, Scheie Eye Institute, Perelman School of Medicine, University of Pennsylvania, Philadelphia, Pennsylvania, USA.*
[†]*Both authors contributed equally to this work.*

To treat patients affected with bestrophinopathies caused by mutations in the *BEST1* gene, a recombinant adeno-associated virus vector (OPGx-BEST1 or rAAV2/2-VMD2-*BEST1*) is being developed. The vector construct includes the human BEST1 cDNA under control of the VMD2/BEST1 promoter and is packaged in an AAV2 capsid. This study evaluated the efficacy and toxicity of OPGx-BEST1 administered by subretinal injection in dogs that were homozygous mutant or compound heterozygotes for 3 naturally occurring mutations in *BEST1*. Twelve BEST1-mutant dogs were divided into 4 groups of 3 animals each, and they received in their left eye a subretinal injection of 0.15 mL of OPGx-BEST1 at 1 of 3 concentrations (9.5×10^9 vector genome [vg]/mL; 3.0×10^{10} vg/mL; or 3.0×10^{11} vg/mL) of OPGx-BEST1, resulting, respectively, in a low (1.4×10^9 vg), high (4.5×10^9 vg), and highest (4.5×10^{10} vg) dose or vehicle control. The right eyes were not injected. Subretinal injections were well tolerated and were not associated with any systemic or ocular toxicity. Electroretinography showed improved rod- and cone-mediated responses in eyes treated with OPGx-BEST1. Noninvasive retinal imaging by optical coherence tomography showed improved structural integrity with a reduction or prevention of appearance of vitelliform lesions and reversal of microdetachments in the retinal areas treated with OPGx-BEST1. These results support the use of OPGx-BEST1 in clinical studies with patients affected with bestrophinopathies and define the no-observed-adverse-effect level at 4.5×10^{10} vg/eye (0.15 mL, 3.0×10^{11} vg/mL).

Keywords: autosomal recessive bestrophinopathy (ARB), best vitelliform macular dystrophy (BVMD), photoreceptor function, gene therapy, IND-enabling study

INTRODUCTION

In the retina, *BEST1* (OMIM#607854) is selectively expressed in the retinal pigment epithelium (RPE), the highly specialized monolayer that supports the function and survival of photoreceptor (PR) cells and serves as the outer blood–retina barrier.[1,2] Bestrophin 1 (BEST1) is a multifunctional, transmembrane calcium-activated chloride channel protein localized to the basolateral membrane of RPE cells.[1,3–5] It has been implicated in anion transport, regulation of calcium signaling, and cell volume.[6–8,9–12] Over 200 distinct human *BEST1* gene mutations have been reported to be causally associated with a group of retinal disorders, termed bestrophinopathies.[13–19] The most common and well-defined bestrophinopathy is a juvenile macular dystrophy called Best vitelliform macular dystrophy (BVMD or Best disease), which shows autosomal dominant inheritance (OMIM#153700). Clinically, the disease first manifests as bilateral vitelliform lesions, predominantly beginning in the macular and paramacular areas.[19–25] A spectrum of molecular and structural alterations at the RPE–PR interface triggers the formation of these vitelliform lesions, which can accumulate lipofuscin, eventually progressing toward PR degeneration and vision loss.[4,22,26–31] Clinical disease has been classified into

*Correspondence: Dr. William A. Beltran, Division of Experimental Retinal Therapies, Department of Clinical Sciences & Advanced Medicine, School of Veterinary Medicine, University of Pennsylvania, Philadelphia, PA, 19014 USA. E-mail: wbeltran@vet.upenn.edu
[†]*Both authors contributed equally to this work.*

DOI: 10.1177/10430342261458076

6 stages,[32] beginning with subclinical pre-vitelliform retinal microdetachments (stage I) that can progress to a vitelliform (stage II), pseudohypopyon (stage III), and vitelliruptive (stage IV) appearance followed by retinal atrophy (stage V) and choroidal neovascularization (stage VI).

Like several other inherited retinal diseases, *BEST1* variants can cause biallelic (recessive) retinal disease in addition to the more common monoallelic BVMD.[16,17] Canonical form of biallelic disease shows an autosomal recessive bestrophinopathy (ARB) phenotype with retinal involvement extending from fovea to midperiphery, demonstrating intraretinal cystic changes and subretinal serous detachments. However, biallelic BEST1 disease with central vitelliform lesions similar to the BVMD has also been described.[33]

In dogs, 3 different naturally occurring mutations in *BEST1* cause a recessive retinal disease called canine multifocal retinopathy (cmr) that shares close similarity with the human BVMD phenotype.[34] Lesions of retinal separation are frequently observed first in the *area centralis* (the canine equivalent to the human foveal/parafoveal area[35]) and subsequently in the mid-peripheral/peripheral retina with disease progressing from stages I through V.[34] The subretinal space between PRs and the RPE is abnormally wide and expands with light exposure.[36] Proof-of-concept studies in this model have shown that a *BEST1* gene augmentation strategy successfully corrects clinically visible subretinal vitelliform lesions as well as diffuse microdetachments.[31] In these preliminary gene therapy studies, the reversal of the obvious clinical lesions and microdetachments following the subretinal delivery of a single-stranded recombinant adeno-associated viral vector (AAV2/2) carrying human *BEST1* cDNA under control of the human VMD2/BEST1 promoter was associated with the extension of RPE microvilli and restoration of the cytoarchitecture at the RPE–PR interface.[31]

With the goal of developing a gene therapy product for patients affected with bestrophinopathies, this Investigational New Drug (IND)-enabling study tested the toxicity and efficacy of a good manufacturing practice (GMP)-grade batch of this AAV2/2-VMD2-*BEST1* vector (OPGx-BEST1, formerly named IC-200) in *BEST1* mutant dogs.

MATERIALS AND METHODS

Test article (OPGx-BEST1/AAV2/2-VMD2-BEST1)

The test article (OPGx-BEST1) was produced by co-transfection of human embryonic kidney 293 cells with 3 plasmids: the transgene plasmid VMD2-*BEST1*, the Rep2Cap2 plasmid, and the helper plasmid pALD-X80. It was subsequently purified by affinity and anion exchange chromatography, followed by cesium chloride ultracentrifugation, concentrated/buffer exchanged against balanced salt solution (BSS), and suspended in 0.001% Poloxamer 188, pH 7.0. The specific vector grade used in this study was a toxicity lot that was made under GMP conditions that were similar to that of the future clinical lot.

Vehicle control article

The vehicle control article consisted of BSS containing 0.001% Poloxamer 188 and pH 7.0 and was prepared by Catalent Maryland, Inc. It was used for dosing the vehicle treatment group and also to dilute OPGx-BEST1 to the concentration required for administration to the test article treatment groups.

Animals

A total of 12 dogs (homozygous mutants or compound heterozygotes for 3 different *BEST1* mutations) with an age ranging from 16 to 194 weeks at the time of dosing were used. Dosing of animals as well as *in vivo* and *ex vivo* data acquisition and analysis were performed in a masked manner. Study day 0 was the day of injection for each animal. All animals were terminated at 13 weeks post injection. A mix of male and female dogs was allocated to each treatment group with the exception of the highest dose group, which consisted only of females due to limited availability of animals.

Studies were carried out in strict accordance with the recommendations in the *Guide for the Care and Use of Laboratory Animals* of the National Institutes of Health, in compliance with the United States Department of Agriculture (USDA)'s Animal Welfare Act, Animal Welfare Regulations, and the Association for Research in Vision and Ophthalmology (ARVO) Statement for the Use of Animals in Ophthalmic and Vision Research. The protocols were approved by the Institutional Animal Care and Use Committee of the University of Pennsylvania (IACUC# 803254). The dogs were bred and maintained at the University of Pennsylvania Retinal Disease Studies Facility. This IND-enabling study conducted by the Division of Experimental Retinal Therapies (ExpeRTs) was designed in a manner that addressed the key components of the principles of Good Laboratory Practice (GLP) regulations as set forth in 21 CFR Part 58, GLP for Nonclinical Laboratory Studies, which included the involvement of quality control and quality assurance units throughout the duration of the study but was not formally fully GLP compliant.

For a comprehensive description of the methods, including subretinal injection, medication regimen, and in-life and postmortem toxicology and efficacy assessment, including statistical analysis, see Supplementary Data and previously published methodologies.[31,37,38]

RESULTS AND DISCUSSION

Relevance for clinical trials

Results of this study supported a clinical trial in which patients with BVMD or ARB caused by mutation in *BEST1* are receiving OPGx-BEST1 administered by subretinal injection. The clinical trial is a Phase 1b/2a, open-label, dose-exploring, safety, and tolerability study. Details are available at https://clinicaltrials.gov/study/NCT07185256.

Objective and study design

The study was designed to evaluate the toxicity and efficacy of OPGx-BEST1 administered by subretinal injection in *BEST1*-mutant dogs. The subretinal surgical procedure in the first 9 animals was performed over 3 consecutive days. On each day, both doses (high, low) of the test article and the vehicle were administered in the left eye (LE) of 3 different animals. To ensure similar representation in gender, ages, stages of disease, and genotypes, the animals were preassigned in a non-randomized manner to the different treatment groups. Three animals received a subretinal injection of OPGx-BEST1 at the high-dose (150 µL, 3.0×10^{10} vg/mL, 4.5×10^{9} vg/eye, high-dose group). Three animals received a subretinal injection of OPGx-BEST1 at the low-dose (150 µL, 9.5×10^{9} vg/mL, 1.4×10^{9} vg/eye, low-dose group), and 3 animals received a subretinal injection of the vehicle control article (150 µL, Alcon BSS with 0.001% Poloxamer 188, vehicle group). After completion of this initial study, 3 additional mutant BEST1 dogs were added to test a higher dose (150 µL, 3.0×10^{11} vg/mL, 4.5×10^{10} vg/eye, highest-dose group) of the test article OPGx-BEST1. The right eyes (RE) of all 12 dogs remained untreated. At the time of surgery, visualization through the operating microscope of the formation of a large subretinal bleb (Fig. 1A2–D2) immediately following the injection was the criteria for retaining dogs in the study. As all dogs were successfully injected, they were all retained in the study and followed for 13 weeks post treatment, at which point they were euthanized for histopathological analysis. An outline of the study design can be found in Table 1 and Supplementary Table S1.

Summary of data

1. Clinical observations. Daily clinical observations did not reveal any systemic toxicity associated with the test article. Comparison of body weights across treatment groups throughout the in-life portion of the study did not show any effect of the test article. All animals reached the end of the study (week 13) with good body condition.

2. Ophthalmic examinations. BEST1-associated lesions observed by indirect ophthalmoscopy and confocal scanning laser ophthalmoscopy (cSLO) were staged,[34] and their progression in the treated area of the injected eyes was compared with the progression of lesions observed in the untreated area of the injected eyes and equivalent treated area of the contralateral non-injected eyes. Note: the earliest stage that can be diagnosed by funduscopic examination or cSLO imaging is stage II (vitelliform lesion).

Ophthalmic findings in the 12 non-injected eyes (Supplementary Table S2) showed persistence or lesion appearance in 8 out of 12 eyes. Persisting lesions in the treated area were also observed in the 1 out of 3 vehicle-injected eyes (Supplementary Table S3; Fig. 1A1–A3).

Ophthalmic findings in the 3 eyes that were injected with the low dose of OPGx-BEST1 are summarized in Supplementary Table S4. In the single eye from this treatment group that had funduscopically visible lesions (stage III) at pre-dose, lesions persisted in the untreated area but were less pronounced and appeared to have reverted more to a stage II appearance in the treated area (Fig. 1B1–B3). No lesions appeared in the 2 remaining eyes. Thus, evidence for some potential efficacy of low-dose OPGx-

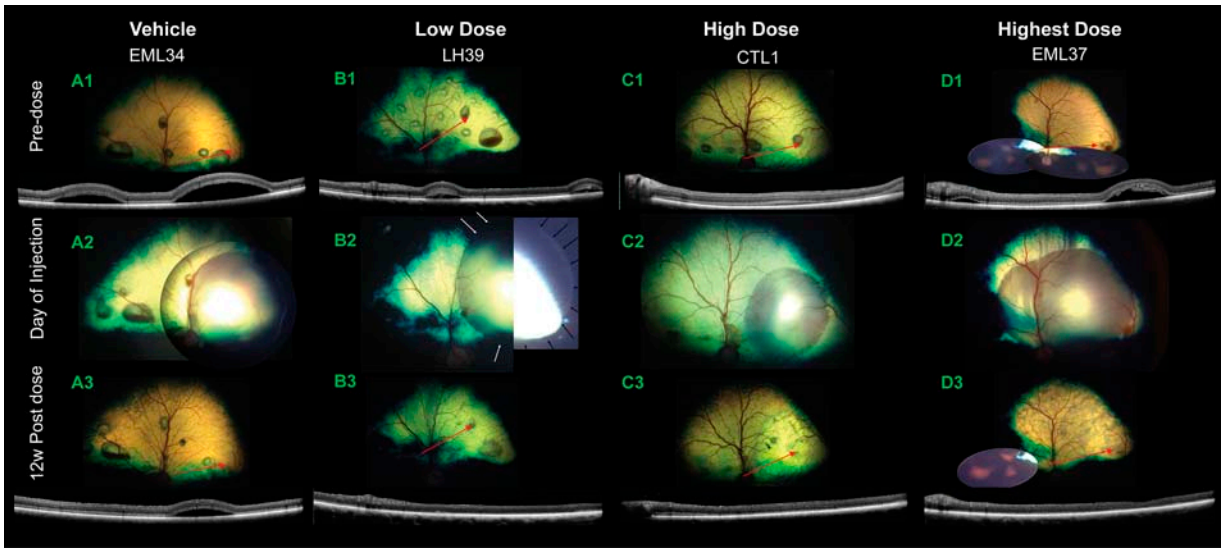

Figure 1. Retinal imaging from selected dogs of all treatment groups illustrating the location and appearance of the treated retinal area prior to, immediately after, and 12 weeks post dosing. **(A1–D1)** Color fundus photographs and optical coherence tomography (OCT) images performed before dosing (*left eyes*). All treatment groups display multiple Stage II/III lesions (**D1** is a photomontage). **(A2–D2)** Subretinal blebs immediately after subretinal injection of vehicle or test article OPGx-BEST1 **(A2** and **B2** are photomontages). **(A3–D3)** Fundus appearance 12 weeks post-dose. Red arrow on fundus photographs indicates the location of the single OCT b-scan shown below.

Table 1. *Study Design to Evaluate Subretinal Injection of OPGx-BEST1 in BEST1 Mutant Dogs*

				Dosage level		
Group	*No. of animals*	*Dog ID sex (age at dosing in weeks)*	*BEST1 genotype*	*Vector concentration (vg/mL)*	*Total dose (vg per eye)*	*Injection volume (mL)*
Highest	3	EMC18 F (113)	cmr1/cmr1	3.0×10^{11}	4.5×10^{10}	~0.15
		EML36 F (113)	cmr1/cmr3			
		EML37 F (113)	cmr1/cmr3			
High	3	CT5 M (17)	cmr2/cmr2	3.0×10^{10}	4.5×10^{9}	~0.15
		CTL1 M (72)	cmr2/cmr3			
		EML35 F (16)	cmr1/cmr3			
Low	3	CTL3 M (17)	cmr2/cmr3	9.5×10^{9}	1.4×10^{9}	~0.15
		ECT2 F (49)	cmr1/cmr2			
		LH39 M (108)	cmr3/cmr3			
Vehicle	3	CT4 M (17) EML34 M (93)	cmr2/cmr2	0 (control)	0	~0.15
		LH37 F (194)	cmr1/cmr3			
			cmr3/cmr3			

Each animal received a subretinal injection in the left eye. The right eye was not injected and served as control.
cmr, canine multifocal retinopathy.
Numbering refers to the specific canine BEST1 mutation.

BEST1 could be detected in 1 out of 3 dogs. In one animal, the retina in the treated area had not fully reattached by 1 week post dose. In this area, a localized site of hyperreflectivity and retinal folds was seen that persisted until 12 weeks post dose. This could have been caused by the surgical procedure and thus cannot be unambiguously related to the test article. No clinical signs of toxicity were seen in the other 2 of 3 low-dose OPGx-BEST1-injected eyes.

Ophthalmic findings in the 3 eyes that were injected with the high dose of OPGx-BEST1 are summarized in Supplementary Table S5. In one eye, a single focal stage III lesion detected at pre-dose in the treated area disappeared following treatment (Fig. 1C1–C3), yet all stage II and III lesions in the untreated area persisted. In another eye, no lesions developed in the treated area, yet numerous multifocal Stage II lesions appeared at 8 weeks post-dose in the untreated area. Finally, no lesions appeared in the third eye. Thus, evidence for some potential efficacy of high-dose OPGx-BEST1 could be detected in 2 out of 3 dogs. No clinical signs of toxicity were seen in any of the high-dose OPGx-BEST1-injected eyes, and ocular findings were related either to the surgical procedure or to natural course of disease in this model.

Ophthalmic findings in the 3 eyes injected with the highest dose of OPGx-BEST1 are summarized in Supplementary Table S6. One eye had a stage II lesion at baseline, which was treated and resolved from the 1-week post-dosage timepoint onwards. Stage III lesions that were noted in 2 dogs pre-dosing all resolved by the end of the study (Fig. 1D1–D3). Areas of mottled gray coloration with reduced tapetal reflectivity were seen in the bleb/injected region of all 3 eyes (Fig. 1D3). These observations were not considered adverse events, as these changes could not be associated with any detectable signs of structural alterations by optical coherence tomography (OCT) nor on histological sections.

In summary, ophthalmoscopic evidence of a positive therapeutic effect was observed in some dogs across all OPGx-BEST1 treatment groups. Most of the other ophthalmic findings (*e.g.,* conjunctival hyperemia, retinotomy, retinal folds) seen in the injected eyes across all treatment groups were observed postoperatively and considered to be related to either the surgical procedure or the medication regimen (subconjunctival injection of triamcinolone acetonide). No such findings were seen in the contralateral non-injected eyes.

3. Quantification of retinal structure *in vivo*. Canine BEST1 disease is defined by the following 3 anatomical features detectable by *in vivo* imaging: large vitelliform separations of the RPE from PR, microdetachment at the level of RPE–PR interface, and loss of PR cells by thinning of the outer nuclear layer (ONL). Two different approaches using standard resolution OCT-derived maps (Fig. 2; Supplementary Figs. S1–S3) and single high-resolution (HR) OCT B-scans (Supplementary Fig. S4) allowed independent assessment of the effect of treatment on preservation of the ONL thickness and restoration of the RPE–PR interface (OS+ thickness).

OCT map analysis of OS± thickness. Qualitative analysis of OS+ thickness on OCT maps revealed a positive treatment effect (reduction of the RPE–PR distance) that was limited to the treated area of eyes injected with the low, high, and highest doses (Supplementary Fig. S2). No such effect was seen in any of the vehicle-injected eyes. However, in the contralateral non-injected eyes (Supplementary Fig. S3), although multifocal retinal lesions persisted or appeared, pan-retinal reduction in OS+ thickness was seen when comparing the pre-dose with the 12-week post-dose timepoint in 3 out of 3 dogs from the highest dose group and in 1 out of 3 dogs in the vehicle, low, and high dose groups.

When compared with the pre-dose timepoint, OS+ thickness in the treated areas of the eyes injected with the test

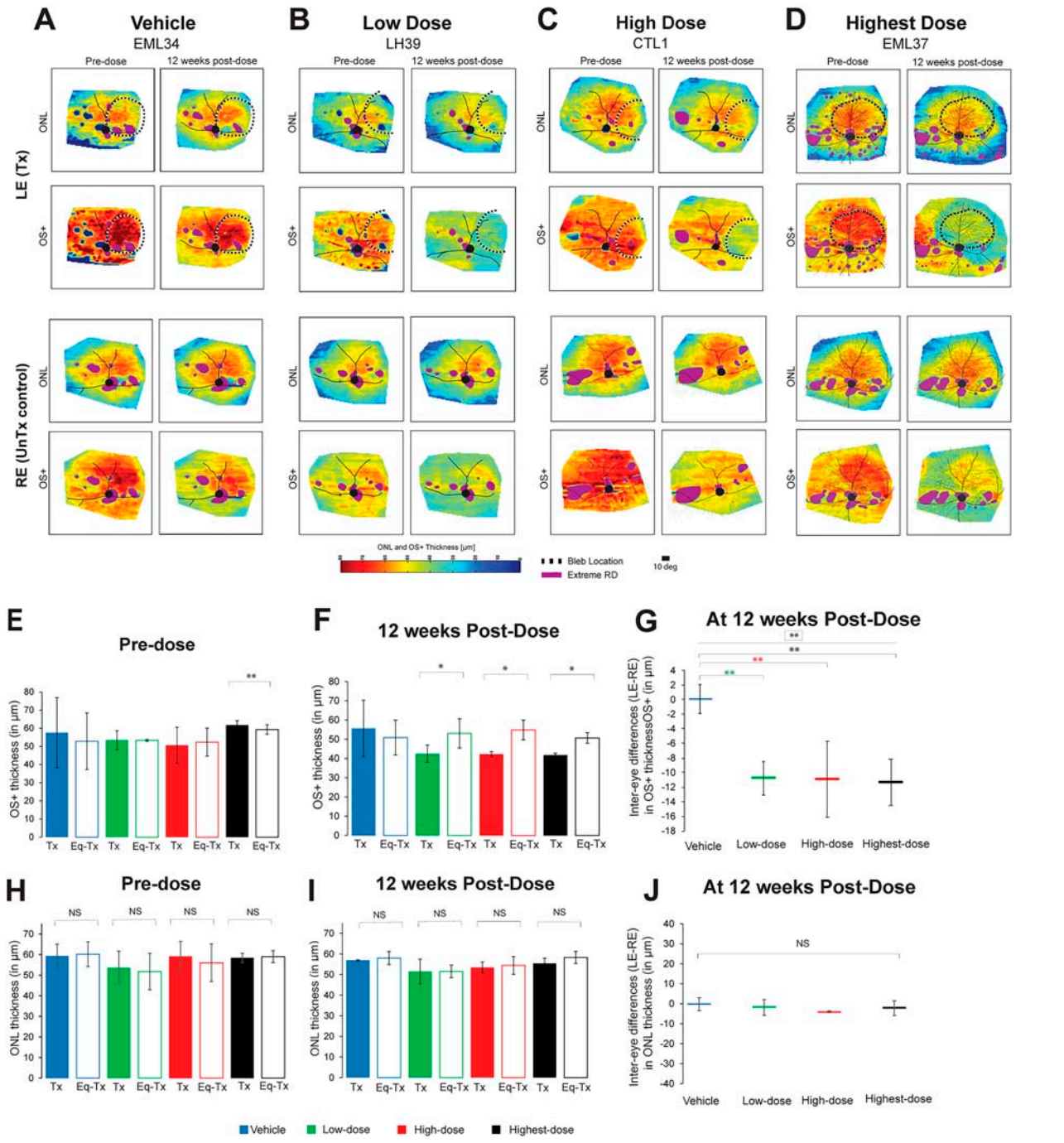

Figure 2. *In vivo* assessment of outer nuclear layer and RPE–photoreceptor interface thickness at pre-dose and 12 weeks post-treatment by optical coherence tomography imaging. **(A–D)** Representative pseudocolor maps showing ONL and RPE–photoreceptor (=OS+) thickness of the injected LE and non-injected right eye (RE) of 1 dog from each dosage group at pre-dose and 12 weeks post-dose. Treatment boundaries are based on fundus photographs of the bleb taken at the time of the injection (*dotted lines*). Optic nerve and major blood vessels (*black*) are overlaid for ease of comparison. **(E)** Inter-eye comparison within treatment groups of the mean (±SD) OS+ thickness in the treated area of the injected (LE) eyes and the equivalent treated areas of the non-injected/contralateral RE at pre-dose. Analyzed by paired *t*-test. **(F)** Inter-eye comparison within treatment groups of the mean (±SD) OS + thickness in the treated area of the injected (LE) eyes and the equivalent treated areas of the non-injected/contralateral) eyes (RE) at 12 weeks post dose. Paired *t*-test: *= $p \leq 0.05$. **(G)** Comparison across treatment groups of the normalized inter-eye difference [IED (LE–RE) at 12 weeks—IED (LE–RE) at pre-dose]. Boxed asterisks represent p values from the one-way ANOVA; colored asterisks represent p values of the Bonferroni *post hoc* analysis: NS = non-significant, *= $p \leq 0.05$, **= $p \leq 0.01$. **(H)** Inter-eye comparison within treatment groups of the mean (±SD) ONL thickness in the treated area of the injected (LE) eyes and the equivalent treated areas of the non-injected/contralateral eyes (RE) at pre-dose. Analyzed by paired *t*-test. **(I)** Inter-eye comparison within treatment groups of the mean (±SD) ONL thickness in the treated area of the injected (LE) eyes and the equivalent treated areas of the non-injected/contralateral (RE) eyes at 12 weeks post dose. Analyzed by paired *t*-test. **(J)** Comparison across treatment groups of the normalized inter-eye difference [IED (LE–RE) at 12 weeks—IED (LE–RE) at pre-dose]. Analyzed by one-way ANOVA test. IED, inter-eye differences; ONL, outer nuclear layer; RPE, retinal pigment epithelium.

article was reduced (Fig. 2E, F). In addition, comparison of the OS+ thickness between treated areas of the injected eyes and equivalent areas of the non-injected eyes showed a reduction in all 3 dose groups, which was statistically significant with the low and highest doses (Fig. 2F).

Quantitative comparison across treatment groups of the mean inter-eye differences (IED) in OS+ thickness at 12 weeks post-dose (normalized to the IED at pre-dose) between the treated area of the injected left eyes (LE) and the equivalent treated area of the non-injected contralateral RE showed an overall statistical difference ($p = 0.01$) (Fig. 2G). *Post hoc* comparison showed a statistically significant reduction in the low-dose OPGx-BEST1 (-10.7 ± 2.3 μm; $p = 0.005$), the high-dose OPGx-BEST1 (-10.9 ± 5.2 μm; $p = 0.005$), and the highest-dose OPGx-BEST1 (-11.3 ± 3.2 μm; $p = 0.004$) groups when compared with vehicle (0.0 ± 2.0 μm).

HR OCT single B-scan analysis of OS± thickness. Qualitative evaluation of the HR OCT B scans showed a reduced distance between the inner segment/outer segment (IS/OS) and RPE/T layers in animals from both the low and high dose groups (Supplementary Fig. S4B1 and B2, C1 and C2) when comparing the treated area of the injected eyes (LE) and the equivalent treated area of the non-injected contralateral eyes (RE). This treatment effect was less apparent in the highest dose group (Supplementary Fig. S4D1 and D2) and not observable in the vehicle group (Supplementary Fig. S4A1 and A2). Quantitative comparison across treatment groups of the mean inter-eye differences in OS+ thickness at 12 weeks post-dose between the treated area of the injected eyes (LE) and the equivalent treated area of the non-injected contralateral eyes (RE) showed an overall statistically significant ($p = 0.04$) difference across all dosage groups. *Post hoc* comparison confirmed statistically significant reduction in the low-dose group (-22.6 ± 15.2 μm; $p = 0.008$) and the high-dose group (-17.7 ± 11.8 μm; $p = 0.02$) but not the highest-dose group (-11.4 ± 1.5 μm; $p = 0.07$) when compared with vehicle (5.6 ± 4.6 μm).

In summary, taken together, both independent methods of OCT analysis confirmed that administration of OPGx-BEST1 results in reduction of OS+ thickness across all dosage groups.

OCT map analysis of ONL thickness. No significant differences in ONL thickness were seen within each treatment group between the treated area of the injected eyes and the equivalent area of the contralateral (non-injected) eyes at pre-dose (Fig. 2H) and 12 weeks post-dose (Fig. 2I). Similarly, when interocular difference in ONL thickness was compared across treatment groups at 12-weeks post-dose, no significance was found (Fig. 2J). When examining individual ONL thickness maps (Supplementary Figs. S2 and S3), it was apparent that some individuals from all 4 treatment groups had a reduction in ONL thickness between the pre- and the 12-weeks post dose timepoints (*e.g.,* animals CT4, CTL3, EML35, EML36). However, as this was seen in the treated and untreated areas of the injected eyes and the equivalent areas in the non-injected eyes, this was most likely not related to the test or vehicle articles.

HR OCT single B-scan analysis of ONL thickness. In all 3 dogs of the low, high, and highest groups, ONL thickness in the treated area at 12 weeks post-dose was within the 95% confidence intreval (CI) of normal dogs, except in areas of BEST1-associated focal retinal detachment where the ONL was below the 95% CI. No significant differences were seen when comparing the mean ONL thickness in the treated area of the injected eyes to that of the equivalent treated area of the contralateral non-injected eyes. In 12 out of 12 non-injected eyes, ONL thickness at 12 weeks post-dose was within or slightly above the 95% CI of normal dogs, except in areas of a focal BEST1 lesion with retinal detachment where ONL thinning was seen. A similar finding was observed in all 3 vehicle-injected eyes. Representative images from a dog of each treatment group are shown in Supplementary Fig. S4.

4. Electroretinography. At the pre-dose timepoint, the mean interocular amplitude differences were minimal, and there were no significant differences across treatment groups under conditions that elicit rod, mixed rod-cone, and cone responses (Fig. 3A, C, E, G; Supplementary Fig. S5). At 11 weeks post-dose, an increase in interocular amplitude differences between treated and contralateral non-injected eyes was seen in the low, high, and highest dose groups (Fig. 3B, D, F, H; Supplementary Fig. S5). The most prominent and statistically significant differences in interocular amplitudes following stimulations under scotopic conditions with a range of light intensities were found in the high-dose group (Fig. 3B, D). These results suggest that OPGx-BEST1 improves rod and mixed rod-cone ERG responses. Under photopic conditions that isolated cone-mediated ERG responses (Fig. 3F, H), there was also an increase in interocular amplitude differences in favor of the injected eye in all 3 OPGx-BEST1 treatment groups.

In summary, no signs of retinal toxicity that could be associated with the low-, high-, or highest-dose groups of OPGx-BEST1 were detected by ERG. Results showed, on the contrary, a dose-dependent improvement in ERG responses following treatment with OPGx-BEST1, which was maximized when using the high dose.

5. Clinical pathology. There were no test article-related effects on hematology, coagulation, or clinical chemistry parameters in any of the treatment groups. Any abnormal clinical pathology findings were seen across all groups and were most likely not caused by the administration of OPGx-BEST1. Mild transient liver value elevations and leukocyte elevations were attributed to medication such as corticosteroids administered post dosage,[39] especially since cessation of corticosteroids resulted in a

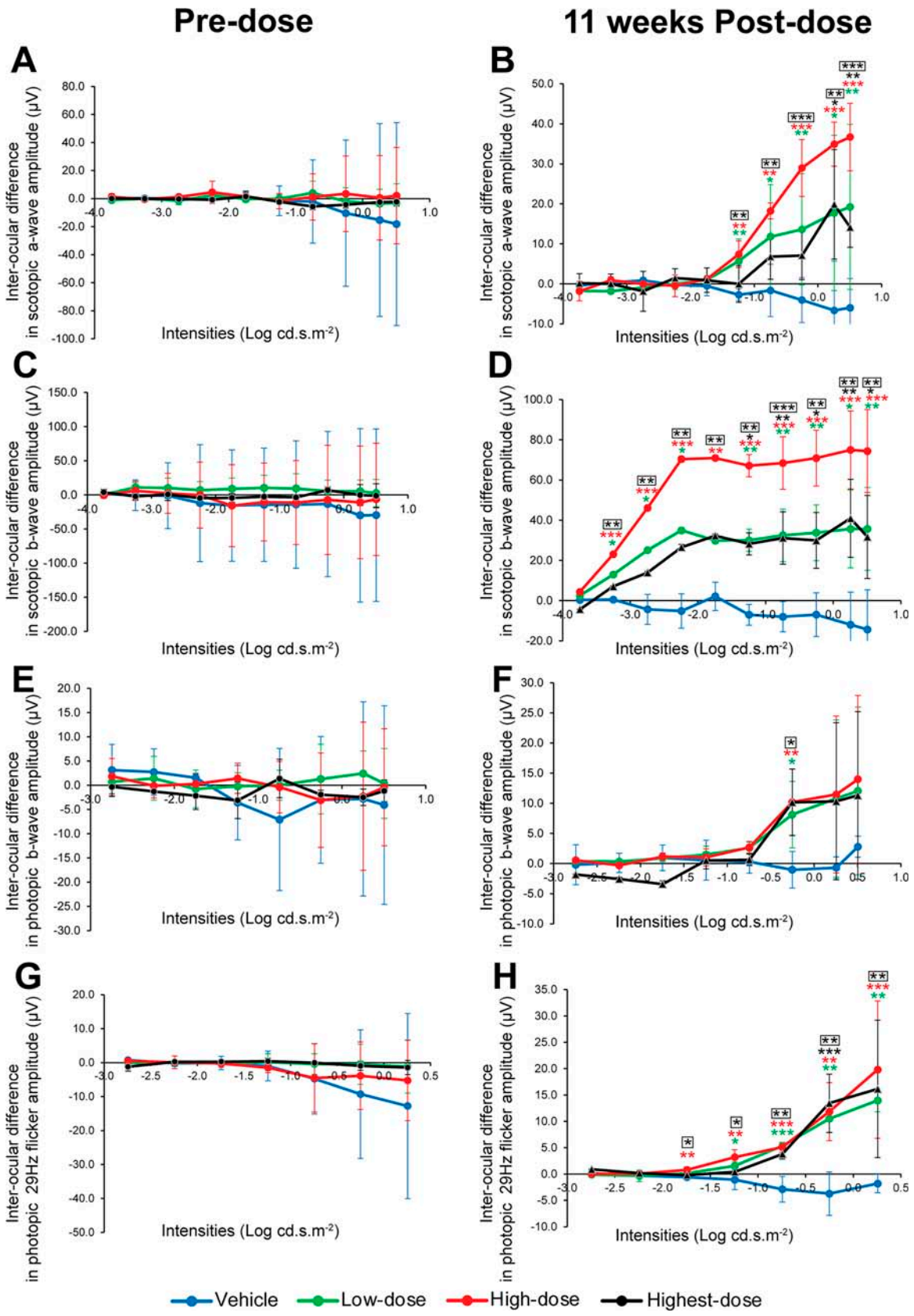

Figure 3. Comparison of full-field ERG amplitudes across treatment groups at pre-dose and 11 weeks post-dose. Mean (±SD) interocular differences in scotopic a-wave **(A, B)**, scotopic b-wave **(C, D)**, photopic b-wave **(E, F)**, and 29-Hz flicker **(G,H)** amplitudes between the injected left eyes eyes and non-injected right eyes as a function of intensity of light stimulus (in Log cd. s. m-2). Boxed asterisks represent *p* values from the one-way ANOVA; colored asterisks represent *p* value of Bonferroni *post hoc* analysis: *= $p < 0.05$, **= $p \leq 0.01$, and ***= $p \leq 0.001$.

reversal of these abnormalities. Other transient abnormalities were attributed to the sampling process itself—physical restraint likely caused elevated creatinine kinase levels[40,41] in 2 dogs at separate timepoints, while focal cases of mild increases in reticulocyte counts. No clinically relevant coagulation abnormalities were noted. All anomalous clinical pathology results were deemed unremarkable by a board-certified veterinary clinical pathologist.

6. Non-ocular histopathology. There were no test article-related effects on organ weights. None of the gross pathology and histopathological findings were obviously test-article related. Most dogs exhibited axonal degeneration in the optic nerves and optic tracts, characterized by dilated myelin sheaths, swollen and hyper-eosinophilic axons (spheroids), and/or myelinomacrophages within digestion chambers. These changes remained minimal and were often seen bilaterally throughout all experimental groups, including the vehicle-injected group. The cause for the axonal degeneration is difficult to ascertain and may have been caused by the focal retinal disruption at the site of retinotomy.

In the highest dose group, 2 dogs showed multifocal mild epicardial discoloration of the right atrium of unknown significance. No cardiac-related clinical signs were reported in these dogs, and histopathological examination of cardiac tissue revealed changes reminiscent of atrial myocarditis.[42] While transient myocarditis has been reported in humans following AAV gene therapies, most cases are reported within 1–3 weeks post-treatment and are associated with doses greater than 1×10^{13} vector genomes per kilogram body weight, which is far higher than the highest dose used in this experiment (4.5×10^{10} vg in total).[43] In addition, AAV vectors commonly associated with myocarditis[43] do not include the one used in the present study (rAAV2/2) that has a known tropism for PRs and RPE when delivered subretinally.[44–46] In summary, regarding this poorly understood inflammatory condition, a test article-related effect is unlikely but not fully ruled out.

7. Ocular histopathology. No histological evidence of intraocular hemorrhage, inflammation, or necrosis was observed in any of the injected or non-injected eyes. Significantly, no signs of ocular toxicity toward the viral vector could be seen within all 3 OPGx-BEST1 dosage groups (Fig. 4A). All injected eyes in the treatment groups showed preservation of the ONL and inner and outer segments in the treated area, with a mean ONL thickness that was comparable with that of the equivalent area of the non-injected contralateral eyes (Fig. 4B,C; Supplementary Fig. S6). There was no significant difference in the mean interocular (treated vs contralateral non-injected) ONL thickness across treatment groups (Fig. 4D). The few cases of ocular abnormalities that were observed included focal retinal detachments with RPE hypertrophy and occasional accumulation of RPE cytoplasmic lipofuscin—all commonly seen lesions associated with BEST1 disease itself. Absence of test article-induced retinal toxicity observable via light microscopy was seen even in the highest dosage group.

8. Viral vector shedding and biodistribution. A validated qPCR assay performed on fluids collected throughout the study and on tissues sampled postmortem revealed dose-dependent levels of OPGx-BEST1 within the aqueous humor of the treated eyes at 4 weeks post-dose. OPGx-BEST1 remained detectable until week 13, although the copy numbers were lower than at week 4, pointing toward a decrease in OPGx-BEST1 concentration in the aqueous humor over time (Supplementary Fig. S7). Low positive signals were detected in the bulbar conjunctiva, optic nerve, tears, spleen, and saliva of dogs injected with OPGx-BEST1. All other tissue samples contained no detectable levels of OPGx-BEST1.

9. Immunological studies. Mean total blocking antibody titers (expressed as inverse of greatest dilution) directed against AAV2 from animals of each treatment group are shown in Figure 5. While low titers were observed at pre-dose and post-dose in both vehicle-, low-dose-, and high-dose-injected animals, a prominent increase in total blocking antibody titers directed against AAV2 was seen at 8 weeks post-dose in the highest dose group, and levels persisted until termination.

CONCLUSIONS

This IND-enabling study in a naturally-occurring canine model evaluated the efficacy and toxicity of an

Figure 4. Representative retinal histology and quantification of ONL thickness at 13 weeks post dose in individual injected and non-injected eyes from all 3 treatment groups. **(A)** Photomicrographs of hematoxylin-eosin (H&E)-stained sections showing the retinal morphology in the treated area of the injected (LE) eye and the equivalent location of the contralateral non-injected (RE) eye. **(B)** Spidergraphs of ONL thicknesses measured in both eyes (*green traces* = LE/injected eye; *red traces* = RE/non-injected eye) that extend from the optic nerve head (ONH) to the peripheral ora serrata along both the inferonasal (Inf.-Nasal) and superotemporal (Sup. – Temp.) quadrants. The section was oriented to include the treated area in LE and equivalent area in RE. The blue bar above the *x*-axis of each spidergraph corresponds to 5 locations within the treated area (and equivalent area in RE) that were selected for calculation of the mean ONL thickness in the treated area of LE and equivalent area in RE. The black arrows point to the location of the photomicrographs. **(C)** Quantitative analysis of the retention of ONL thickness in the treated area measured by histology at 13 weeks post-dose. Mean (±SD) ONL thickness of the treated area of the injected (LE) eyes and of the equivalent area of the non-injected (RE) eyes in the vehicle, low-dose, and high-dose treatment groups. Paired *t*-tests; NS = non-significant **(D)** Comparison across treatment groups of the mean (±SD) difference in ONL thickness between the treated area of the injected (LE) eyes and the equivalent area of the non-injected (RE) eyes. One-way ANOVA; NS = non-significant.

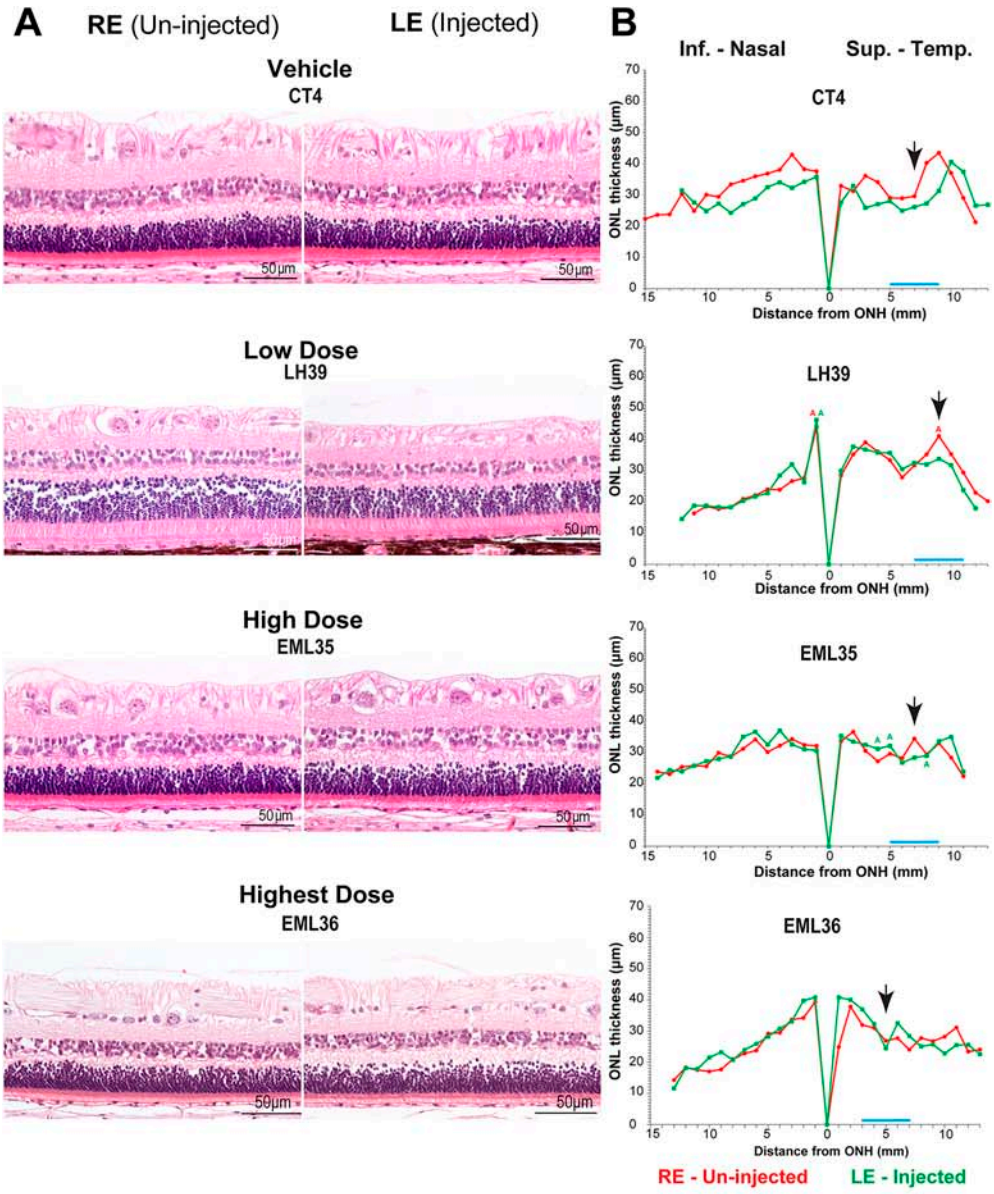
A
RE (Un-injected)
LE (Injected)
Vehicle
CT4
Low Dose
LH39
High Dose
EML35
Highest Dose
EML36
50µm
B
Inf. - Nasal
Sup. - Temp.
CT4
LH39
EML35
EML36
ONL thickness (µm)
Distance from ONH (mm)
RE - Un-injected
LE - Injected
C
ONL thickness (µm)
NS
Vehicle - Injected
Vehicle - Uninjected
Low dose - Injected
Low dose - Uninjected
High dose - Injected
High dose - Uninjected
Highest dose - Injected
Highest dose - Uninjected
D
Inter-eye differences (LE-RE) in ONL thickness (in µm)
Vehicle
Low dose
High dose
Highest dose

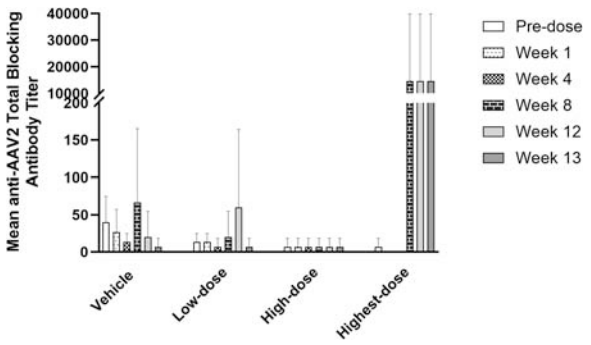

Figure 5. Serum titers of total blocking antibodies directed against AAV2 capsid proteins. Antibody titers (mean ± SD) measured in serum collected at baseline (pre-dose), 1, 4, 8, 12, and 13 weeks post-dose from all dogs of the 4 treatment groups.

AAV-based gene therapy (OPGx-BEST1) developed for the treatment of bestrophinopathies in human patients. *In vivo* OCT imaging and ERG analysis showed evidence of restoration of the PR to RPE interface and improved retinal function following subretinal injection of the low-, high-, and highest doses of OPGx-BEST1 when compared with vehicle. However, we observed that the interocular differences in scotopic ERG a- and b-wave amplitudes were most pronounced in the high-rather than in the highest-dose group. Although we cannot exclude the possibility that this non-monotonic (bell-shaped) dose response could be due to saturation of the cellular translational machinery at high multiplicity of infection,[47] the most plausible cause for this result is that subretinal blebs in all 3 eyes from the highest dose covered a smaller retinal surface than that achieved in the eyes of the high-dose group. No signs of toxicity associated with OPGx-BEST1 were detected by clinical assessment, histology, and clinical pathology for up to 13 weeks post injection in any of the dosage groups. While a significant elevation in the titers of AAV2 total blocking antibody occurred as early as 8 weeks post injection in the highest dose group, several publications have shown that production of systemic anti-AAV2 antibodies in dogs, nonhuman primates, and in RPE65-LCA2 patients does not impede or neutralize AAV-mediated expressions or therapeutic effect when the same vector construct is administered subretinally 15 days to years later to the contralateral eye.[48–50] Based on these study results, the no-observed adverse effect limit of OPGx-BEST1 is 4.5×10^{10} vg/eye (0.15 mL, 3.0×10^{11} vg/mL) in naturally occurring *BEST1*-mutant dogs. This study supports the use of OPGx-BEST1 in clinical studies with patients affected by bestrophinopathies caused by *BEST1* gene mutations.

ACKNOWLEDGMENTS

The authors thank Jacqui Wivel and the RDSF staff for canine husbandry and assistance in all in-life studies and Lydia Melnyk for research coordination.

AUTHORS' CONTRIBUTIONS

A.V.C., G.D.A., and W.A.B. designed the experiments. A.G., J.C.K, Y.S., C-A.A., and W.A.B. performed the experiments. A.G., J.C.K., and W.A.B. interpreted the data and wrote the article. All the authors read and approved the final article.

AUTHOR DISCLOSURE STATEMENT

A.V.C., G.D.A., and W.A.B. are coinventors on a patent application related to this work. M.C. and A.J. are employees of Opus Genetics, Inc.

FUNDING INFORMATION

This work was supported by Sponsored Research Agreements from Iveric Bio, Inc. and Opus Genetics, Inc. to the University of Pennsylvania; research grants from NIH/National Eye Institute (R01-EY006855, P30-EY001583); and from the Foundation Fighting Blindness.

SUPPLEMENTARY MATERIAL

Supplementary Figures
Supplementary Tables
Supplementary Data

REFERENCES

1. Marmorstein AD, Marmorstein LY, Rayborn M, et al. Bestrophin, the product of the Best vitelliform macular dystrophy gene (VMD2), localizes to the basolateral plasma membrane of the retinal pigment epithelium. Proc Natl Acad Sci U S A 2000;97(23):12758–12763.
2. Strauss O. The retinal pigment epithelium in visual function. Physiol Rev 2005;85(3):845–881.
3. Sun H, Tsunenari T, Yau KW, et al. The vitelliform macular dystrophy protein defines a new family of chloride channels. Proc Natl Acad Sci U S A 2002;99(6):4008–4013.
4. Gómez NM, Tamm ER, Straußβ O. Role of bestrophin-1 in store-operated calcium entry in retinal pigment epithelium. Pflugers Arch 2013;465(4): 481–495.
5. Johnson AA, Guziewicz KE, Lee CJ, et al. Bestrophin 1 and retinal disease. Prog Retin Eye Res 2017;58:45–69.
6. Rosenthal R, Bakall B, Kinnick T, et al. Expression of bestrophin-1, the product of the VMD2 gene, modulates voltage-dependent Ca2+ channels in retinal pigment epithelial cells. Faseb J 2006;20(1):178–180.

7. Hartzell HC, Qu Z, Yu K, et al. Molecular physiology of bestrophins: Multifunctional membrane proteins linked to best disease and other retinopathies. Physiol Rev 2008;88(2):639–672.
8. Strauß O, Müller C, Reichhart N, et al. The role of bestrophin-1 in intracellular Ca(2+) signaling. Adv Exp Med Biol 2014;801:113–119.
9. Kane Dickson V, Pedi L, Long SB. Structure and insights into the function of a Ca(2+)-activated Cl(-) channel. Nature 2014;516(7530):213–218.
10. Yang T, Liu Q, Kloss B, et al. Structure and selectivity in bestrophin ion channels. Science 2014;346(6207):355–359.
11. Yang T, Justus S, Li Y, et al. BEST1: The Best Target for Gene and Cell Therapies. Mol Ther 2015;23(12):1805–1809.
12. Milenkovic A, Brandl C, Milenkovic VM, et al. Bestrophin 1 is indispensable for volume regulation in human retinal pigment epithelium cells. Proc Natl Acad Sci U S A 2015;112:E2630–E2639.
13. Petrukhin K, Koisti MJ, Bakall B, et al. Identification of the gene responsible for Best macular dystrophy. Nat Genet 1998;19(3):241–247.
14. Seddon JM, Afshari MA, Sharma S, et al. Assessment of mutations in the Best macular dystrophy (VMD2) gene in patients with adult-onset foveomacular vitelliform dystrophy, age-related maculopathy, and bull's-eye maculopathy. Ophthalmology 2001;108(11):2060–2067.
15. Yardley J, Leroy BP, Hart-Holden N, et al. Mutations of VMD2 splicing regulators cause nanophthalmos and autosomal dominant vitreoretinochoroidopathy (ADVIRC). Invest Ophthalmol Vis Sci 2004;45(10): 3683–3689.
16. Schatz P, Klar J, Andreasson S, et al. Variant phenotype of Best vitelliform macular dystrophy associated with compound heterozygous mutations in VMD2. Ophthalmic Genet 2006;27(2):51–56.
17. Burgess R, Millar ID, Leroy BP, et al. Biallelic mutation of BEST1 causes a distinct retinopathy in humans. Am J Hum Genet 2008;82(1):19–31.
18. Davidson AE, Millar ID, Urquhart JE, et al. Missense mutations in a retinal pigment epithelium protein, bestrophin-1, cause retinitis pigmentosa. Am J Hum Genet 2009;85(5):581–592.
19. Boon CJ, Klevering BJ, Leroy BP, et al. The spectrum of ocular phenotypes caused by mutations in the BEST1 gene. Prog Retin Eye Res 2009;28(3):187–205.
20. Best F. Uber eine hereditare Maculaaffektion. Z Augenheilk 1905;13:199–212.
21. Gass JDM. Best's Disease. In: Stereoscopic Atlas of Macular Diseases: A Funduscopic and Angiographic Presentation. C.V. Mosby Co., St. Louis, MO; 1997; pp. 304–311.
22. Pianta MJ, Aleman TS, Cideciyan AV, et al. In vivo micropathology of Best macular dystrophy with optical coherence tomography. Exp Eye Res 2003;76(2):203–211.
23. Bitner H, Schatz P, Mizrahi-Meissonnier L, et al. Frequency, genotype, and clinical spectrum of best vitelliform macular dystrophy: Data from a national center in Denmark. Am J Ophthalmol 2012;154(2):403–412.e4. e404.
24. Pasquay C, Wang LF, Lorenz B, et al. Bestrophin 1–Phenotypes and Functional Aspects in Bestrophinopathies. Ophthalmic Genet 2015;36(3):193–212.
25. Cideciyan AV, Jacobson SG, Swider M, et al. Photoreceptor function and structure in autosomal dominant vitelliform macular dystrophy caused by BEST1 mutations. Invest Ophthalmol Vis Sci 2022;63(13):12.
26. Bakall B, Radu RA, Stanton JB, et al. Enhanced accumulation of A2E in individuals homozygous or heterozygous for mutations in BEST1 (VMD2). Exp Eye Res 2007;85(1):34–43.
27. Yu K, Qu Z, Cui Y, et al. Chloride channel activity of bestrophin mutants associated with mild or late-onset macular degeneration. Invest Ophthalmol Vis Sci 2007;48(10):4694–4705.
28. Guziewicz KE, Slavik J, Lindauer SJ, et al. Molecular consequences of BEST1 gene mutations in canine multifocal retinopathy predict functional implications for human bestrophinopathies. Invest Ophthalmol Vis Sci 2011;52(7):4497–4505.
29. Duncker T, Greenberg JP, Ramachandran R, et al. Quantitative fundus autofluorescence and optical coherence tomography in best vitelliform macular dystrophy. Invest Ophthalmol Vis Sci 2014;55(3):1471–1482.
30. Guziewicz KE, Sinha D, Gomez NM, et al. Bestrophinopathy: An RPE-photoreceptor interface disease. Prog Retin Eye Res 2017;58:70–88.
31. Guziewicz KE, Cideciyan AV, Beltran WA, et al. BEST1 gene therapy corrects a diffuse retina-wide micro-detachment modulated by light exposure. Proc Natl Acad Sci U S A 2018;115:E2839–E2848.
32. Koushik Tripathy BS. Best Disease. StatPearls Publishing; 2023.
33. Cideciyan AV, Jacobson SG, Sumaroka A, et al. Photoreceptor function and structure in retinal degenerations caused by biallelic BEST1 mutations. Vision Res 2023;203:108157.
34. Aguirre GD, Beltran WA. Canine Best disease as a translational model. Eye (Lond) 2025;39(3):412–417.
35. Beltran WA, Cideciyan AV, Guziewicz KE, et al. Canine retina has a primate fovea-like bouquet of cone photoreceptors which is affected by inherited macular degenerations. PLoS One 2014;9(3):e90390.
36. Wu V, Swider M, Sumaroka A, et al. Retinal response to light exposure in BEST1-mutant dogs evaluated with ultra-high resolution OCT. Vision Res 2024;218:108379.
37. Beltran WA, Cideciyan AV, Iwabe S, et al. Successful arrest of photoreceptor and vision loss expands the therapeutic window of retinal gene therapy to later stages of disease. Proc Natl Acad Sci U S A 2015;112(43):E5844–E5853.
38. Dufour VL, Cideciyan AV, Ye GJ, et al. Toxicity and efficacy evaluation of an adeno-associated virus vector expressing codon-optimized RPGR delivered by subretinal injection in a canine model of X-linked Retinitis Pigmentosa. Hum Gene Ther 2020;31(3–4):253–267.
39. Yehia S, Abdou O, Kelany M, et al. Ultrasonographic, morphologic and biochemical alterations in experimentally induced steroid hepatopathy in dogs. Glob Vet 2013;11:123–130.
40. Hall RL, Everds NE. Factors affecting the interpretation of canine and nonhuman primate clinical pathology. Toxicol Pathol 2003;31 Suppl:6–10.
41. Aktas M, Auguste D, Lefebvre HP, et al. Creatine kinase in the dog: A review. Vet Res Commun 1993;17(5):353–369.
42. Wolley R, Blundell R, Else R, et al. Atrial myocarditis as a cause of sinus arrest in a dog. J Small Anim Pract 2007;48:455–457.
43. Maurizi N, Ammirati E, Silver E, et al. Incidence, timing and clinical significance of immune-mediated myocardial injury and myocarditis after gene replacement therapy: A systematic review and meta-analysis. Circ Heart Fail 2026;19(5):e013771.
44. Ali RR, Reichel MB, Thrasher AJ, et al. Gene transfer into the mouse retina mediated by an adeno-associated viral vector. Hum Mol Genet 1996;5(5):591–594.
45. Flannery JG, Zolotukhin S, Vaquero MI, et al. Efficient photoreceptor-targeted gene expression in vivo by recombinant adeno-associated virus. Proc Natl Acad Sci U S A 1997;94(13):6916–6921.
46. Acland GM, Aguirre GD, Ray J, et al. Gene therapy restores vision in a canine model of childhood blindness. Nat Genet 2001;28(1):92–95.
47. Lu Q, Wright A, Pan ZH. AAV dose-dependent transduction efficiency in retinal ganglion cells and functional efficacy of optogenetic vision restoration. Gene Ther 2024;31(11–12):572–579.
48. Amado D, Mingozzi F, Hui D, et al. Safety and efficacy of subretinal readministration of a viral vector in large animals to treat congenital blindness. Sci Transl Med 2010;2(21):21ra16.
49. Annear MJ, Bartoe JT, Barker SE, et al. Gene therapy in the second eye of RPE65-deficient dogs improves retinal function. Gene Ther 2011;18(1):53–61.
50. Bennett J, Ashtari M, Wellman J, et al. AAV2 gene therapy readministration in three adults with congenital blindness. Sci Transl Med 2012;4(120):120ra15.

Received for publication March 12, 2026;
accepted after revision May 18, 2026.

Published online: July 3, 2026.

Supplementary Information (Material and Methods)

Although not fully GLP compliant, this IND-enabling study was designed and conducted in a manner that addressed the key components of the principles of Good Laboratory Practice (GLP) regulations as set forth in 21 CFR Part 58, Good Laboratory Practice for Nonclinical Laboratory Studies. It followed a written pre-approved study protocol with pre-established Standard Operating Procedures (SOPs). Unless stated otherwise, subretinal injections, and all data acquisition and analysis were conducted in a masked manner by all experimenters. Finally, both quality control and quality assurance units were involved throughout the course of the study

Subretinal injections

The OPGx-BEST1 vector or vehicle were administered by a single subretinal injection of 0.15 mL in the left eye (LE) of *BEST1*-mutant dogs. The study initially included the testing of 2 different doses of the OPGx-BEST1 vector (low dose: 9.5 x 10^9 vg/mL in 3 eyes; high dose: 3.0 x 10^{10} vg/mL in 3 eyes), or of the vehicle control (BSS containing 0.001% Poloxamer 188, pH 7.0 in 3 eyes). Following completion of this study, the protocol was amended to add a higher dose group (highest dose: 3.0 x 11^{11} vg/mL in 3 eyes). The contralateral right eyes (RE) remained untreated. Subretinal delivery was performed via a pressure-controlled transvitreal approach without prior vitrectomy using a commercially-available subretinal injection system (MedOne MicroDose™ Injection kit with 25g/38g PolyTip® cannula) that was connected via a viscous fluid injection line to a vitrectomy unit (Stellaris PC, Bausch & Lomb).

Pre-, peri-, and postoperative medication regimen

On the day prior to surgery, dogs received oral administration of corticosteroids (Prednisone: 1 mg/kg) and antibiotics (Amoxicillin trihydrate/clavulanate potassium 12.5-20 mg/kg) in the morning and afternoon. All dogs were then subject to an 8-week medication course starting from the day of dosing. On the morning of surgery, dogs received oral antibiotics (amoxicillin trihydrate/clavulanate potassium; 12.5-20 mg/kg) and topical antibiotic (gentamicin sulfate solution; 1 drop; Allergan, Irvine, CA), as well as anti-inflammatory agents (prednisone; 1 mg/kg; prednisolone acetate; 1% suspension 1 drop/flurbiprofen 0.03%, 1 drop; Bausch and Lomb, Tampa, FL). Prior to starting the procedure, topical mydriatics were given: atropine sulfate 1% drops (Akorn, Inc. Lake Forest, IL, or Wedgewood Pharmacy, Swedesboro, NJ), tropicamide 1% (Akorn, Inc. Lake Forest, IL), and phenylephrine 10% (Paragon Bioteck, Portland, OR), all at doses of 1 drop 3 times, 30 minutes apart. Immediately after the end of the surgical procedure, a subconjunctival injection of 4 mg of triamcinolone acetonide (Kenalog 40 mg/mL; Bristol-Myers Squibb, Montreal), and topical application of an antibiotic-plus-steroid ointment (NeoPolyDex ointment, ¼ inch strip, consisting of neomycin sulfate 3.5 mg, polymyxin B sulfate 10,000 units and dexamethasone 0.1%; Bausch and Lomb, Bridgewater, NJ) and mydriatic (atropine sulfate 1% ointment, ¼ inch strip; Bausch and Lomb, Bridgewater, NJ) were given in the injected left eye (LE) only. In the afternoon following the procedure, all animals received a second dose of oral antibiotic (amoxicillin trihydrate/clavulanate potassium; 12.5-20 mg/kg) and corticosteroids (prednisone; 1 mg/kg). Topical application of atropine sulfate 1% ointment (¼ inch strip) was applied once daily in the injected eye for 1-week post-injection. Corticosteroid suspension (prednisolone acetate; 1%

suspension; 1 drop) was applied twice daily in the treated eye for 2 weeks post-injection and then once daily for the following 2 weeks. Oral antibiotics (amoxicillin trihydrate/clavulanate potassium; 12.5-20 mg/kg) were given twice daily for 5 weeks. Oral corticosteroids (prednisone) were given twice daily for 2 weeks at a dose of 1 mg/kg, then twice daily for 2 weeks at 0.5 mg/kg, followed by once daily for 2 weeks at a dose of 0.5 mg/kg, before ending with every-other-day dosing for 2 weeks at a dose of 0.5 mg/kg. At 4 weeks post-injection, a second subconjunctival injection of 4 mg of triamcinolone acetonide (Kenalog; 40 mg/mL) was given in the treated eye under topical anesthesia (proparacaine 0.5%; 1 drop; Bausch and Lomb, Bridgewater, NJ) and gentle restraint.

In-life toxicology and efficacy assessment

1. *Cage-side observation, physical examination and body weights*

Animals were observed daily for signs of morbidity/mortality. A physical examination conducted by a veterinarian was performed pre-dose, on the day of injection (study day 0), on study day 1 and weekly thereafter (± 3 days). Weights were recorded at each examination. Abnormal findings, including ocular signs, were recorded.

2. *Ophthalmic examination*

A board-certified veterinary ophthalmologist (WAB) familiar with the clinical phenotype of canine bestrophinopathies performed in-life ophthalmic examinations, including slit lamp biomicroscopy, tonometry, indirect ophthalmoscopy, and fundus photography. Inflammatory changes including changes in ocular media transparency were graded as none, mild, moderate or severe. Examinations were conducted throughout the course of

the study as shown in Suppl. **Table 1**. The examiner was masked to the dose administered to the 1st cohort of dogs (vehicle, low dose, high dose) but not to that of the subsequent cohort of dogs that all received the highest dose of OPGx-BEST1

3. Confocal laser ophthalmoscopy/optical coherence tomography retinal imaging.

Confocal laser ophthalmoscopy (cSLO) and optical coherence tomography (OCT) imaging were performed with a Spectralis HRA/OCT2 (Heidelberg) unit at pre-dose, and at 1, 4, 8, and 12 weeks post-dose. Qualitative assessment of cSLO and single OCT B-scans was performed at all time-points and progression of disease was documented.

At the pre-dose, and 12-week post-dose time-points, more extensive semi-automated segmentation was performed in light-adapted eyes to produce topographical maps of the distance between inner and outer segments (IS/OS) of photoreceptors and the RPE-tapetum (RPE/T) interface (denominated hereafter OS+), as well as topographical maps of outer nuclear layer (ONL) thickness. This was done in test-article injected eyes, vehicle-injected eyes and in the non-injected contralateral eyes as previously reported. Results of ONL and OS+ thicknesses within the OPGx-BEST1 injected/treated area were compared to results from the corresponding retinal location on the contralateral non-injected eyes, and to vehicle-injected eyes.

In addition, ultra-high-resolution (UHR) OCT analysis of treatment effect was assessed in all test-article injected eyes, vehicle-injected eyes, and in the non-injected contralateral eyes. This was performed with a Bioptigen Envisu R2210 OCT unit at the 12-week post dose time point as follows. Each 44^{o} x 44^{o} raster image obtained per eye was registered to the corresponding topographic ONL and OS+ thicknesses maps performed with

standard resolution OCT. In the injected left eyes, a single b-scan was selected for analysis based on the location of the bleb, lesions, treatment related changes so that the selected scan went through the bleb and fovea-like regions (or at least through the visual streak). Major lesions were avoided when possible. An equivalently located b-scan was selected in the non-injected contralateral eyes.

For these continuous outcome measures (ONL thickness by OCT), descriptive analysis included reporting of the mean and SD. To account for potential animal-to-animal variability of ONL thickness, the mean difference between the injected (LE) and non-injected (RE) eyes was calculated for each of the three groups treated with the test article and compared with that of the vehicle-control group. The comparison of means across all treatment groups was performed using one-way ANOVA. Regardless of whether the overall group effect was statistically significant, a pairwise comparison between each active treatment group (low, high, and highest dose) and the vehicle-control group was performed by using the two-sample t-test. Within each treatment group, the paired t-test was performed to compare the means between treated eyes and their untreated fellow eyes. All statistical analyses were performed using SAS v9.4 (SAS Institute, Inc.).

4. Electroretinography

Recordings were conducted at pre-dose and at 11 weeks post-dose utilizing an Espion E3 electroretinography unit (Diagnosys LLC, Lowell, MA). Pupils were dilated with topical atropine sulfate (1%), tropicamide (1%) and phenylephrine (10%). After induction with intravenous propofol, dogs were maintained under general inhalation anesthesia (isoflurane). Full-field flash electroretinography (ERG) was performed on both eyes using a custom-built Ganzfeld dome fitted with the LED stimuli of a Color Dome stimulator

(Diagnosys LLC, Lowell, MA). After 20 minutes of dark adaptation, rod- and mixed rod-cone-mediated responses to white flash stimuli of increasing intensities were recorded. Following 5 minutes of white light adaptation, cone-mediated signals to a series of 1 Hz flashes and to 29.4-Hz flicker stimuli were recorded. Amplitudes of the b-wave of the dark-adapted rod response, of the a- and b-waves of the dark-adapted rod-cone mixed response, and the trough-to-peak amplitudes of the light-adapted single flash and 29.4 Hz flicker stimuli were measured. The results of the OPGx-BEST1 injected eyes were compared to the vehicle-treated eyes, and to the non-injected contralateral eyes.

For the continuous ERG outcome measures (amplitudes of ERG waves) measured at pre-dose and 11 weeks post-dose, descriptive analysis (mean, SD) was performed. To account for potential animal-to-animal variability of ERG amplitudes, the mean difference between the injected (LE) and non-injected (RE) eyes was calculated for each of the four treatment groups. The comparison of means for the inter-eye difference (between injected eye and non-injected fellow eye) across all treatment groups was performed using one-way analysis of variance (ANOVA) followed by a linear trend analysis. When there was a significant difference, post-hoc pairwise comparisons (of the 3 active treatment groups vs. vehicle group) with correction for multiple comparisons were made using the Bonferroni test. For each treatment group, the paired t-test test was performed to compare the means between injected eyes and the non-injected contralateral eyes. All statistical analyses were performed in SAS v9.4 (SAS Institute Inc, Cary, NC).

5. Immunological assays

The purpose of these assays was to determine in canine serum the presence or absence of total blocking antibodies directed against adeno-associated virus serotype 2

(AAV2) proteins. Additionally, the antibody titer was determined in samples that confirmed positive for total blocking antibodies. Serum samples were collected throughout the course of the study as detailed in **Suppl. Table 1** and shipped to the Sponsor's test site for determination of total blocking AAV2 antibody titers.

6. Viral shedding/Biodistribution studies

Samples of biological fluids (blood, urine, saliva, tears, aqueous humor) were collected throughout the course of the study (see **Suppl Table 1**) and stored frozen at -80°C. At the time of sacrifice at 13 weeks post-dosage, additional tissue samples were collected and stored frozen at -80°C until analysis. Quantitative PCR based viral shedding/biodistribution assays were contracted to a CDMO (Charles River Laboratories, Senneville, QC, Canada). The following fluids and tissues were collected and analyzed:

- For viral shedding assay: Aqueous humor (at pre-dose, week 1, 4, and 13 post-dose); blood, saliva, tears, and urine (at pre-dose, week 1, 4, 8, and 13 post-dose).
- For biodistribution assay: bulbar conjunctiva, cerebellum, heart, Jejunum, Kidney, Lacrimal gland, lateral genicular nucleus, cerebral cortex, liver, lymph nodes (mandibular), lung, optic nerve, optic tract, periocular tissue (eyelids), parotid gland, pancreas, skeletal muscle, skin, spleen, ovary, testis (All at 13 weeks post-dose).

7. Clinical pathology

Blood samples for hematology (complete blood count), routine coagulation profile, and clinical chemistry were collected throughout the course of the study (see **Suppl. Table 1**). Analysis was performed at the University of Pennsylvania School of Veterinary Medicine clinical pathology laboratory, and results were reviewed and interpreted by a board-certified veterinary clinical pathologist. For these continuous outcome measures (clinical

pathology values), descriptive analyses (mean, SD) were performed. The comparisons of means across all treatment groups were performed using one-way analysis of variance (ANOVA) followed by linear trend analysis. When there was a significant difference, post-hoc pairwise comparisons (of the 3 active treatment groups vs. vehicle group) with correction for multiple comparisons were made using the Bonferroni test. All statistical analyses were performed in SAS v9.4 (SAS Institute Inc, Cary, NC).

Postmortem toxicology and efficacy assessment

1. Necropsy

Following exsanguination that was performed under general anesthesia, animals were terminated at 13 weeks post-dose with a commercial pentobarbital-based euthanasia solution (Euthasol; Virbac USA) administered via intravenous injection. Necropsies, tissue collection, and histopathological examinations of formalin-fixed/paraffin-embedded/H&E-stained tissues were conducted by a board-certified veterinary pathologist (co-author C-A A) as previously described (Dufour V.L., et al, *Hum. Gene Ther.*, 2020).

Group means and standard deviations (SD) were calculated for terminal body weight (recorded immediately after euthanasia and before exsanguination), organ weight, organ-to-body weight ratios and organ-to-brain weight ratios. The comparisons of means across all groups were performed using one-way analysis of variance (ANOVA) followed by linear trend analysis. When there was a significant difference, post-hoc pairwise comparisons (of the 3 active treatment groups vs. vehicle control group) with correction for multiple

comparisons were made using the Bonferroni test. All statistical analyses were performed in SAS v9.4 (SAS Institute Inc, Cary, NC).

2. Ocular histopathology

Eyes were enucleated a few minutes after euthanasia. Ocular globes with the proximal optic nerve were fixed in an alcohol-Bouin's solution for 72 hours before being transferred to 70% ethanol until paraffin embedding. H&E-stained paraffin sections of the globes that included the optic nerve head were made through the bleb/treated area (or equivalent area in contralateral non-injected eyes) and were digitally scanned (Aperio digital pathology scanner, Leica). Manual measurements of the ONL thickness were performed using the Aperio ImageScope software at regular (1-mm) intervals extending from the edge of the optic nerve head to the *ora serrata*. Linear graphs of ONL thickness were constructed for both eyes, representing measurements acquired in the superior and inferior plane of the previously defined sections. Based on the area of the bleb along the section, the mean ONL thickness was calculated from five (5) locations within the bleb/treated area. Similarly, five (5) equivalent locations were selected in the contralateral (RE) non-injected eyes to calculate the mean ONL thickness in those eyes. To account for potential animal-to-animal variability in ONL thickness, the mean difference between the injected (LE) and non-injected (RE) eyes was calculated for each treatment group and compared using one-way analysis of variance (ANOVA) followed by a linear trend analysis. When a significant difference was found, post-hoc pairwise comparisons (of the 3 active treatment groups vs. vehicle group) with correction for multiple comparisons were made using the Bonferroni test. Within each treatment group, the paired t-test was performed to compare the means between the injected eyes and the non-injected

contralateral eyes. All statistical analyses were performed in SAS v9.4 (SAS Institute Inc, Cary, NC).

Supplementary Figures

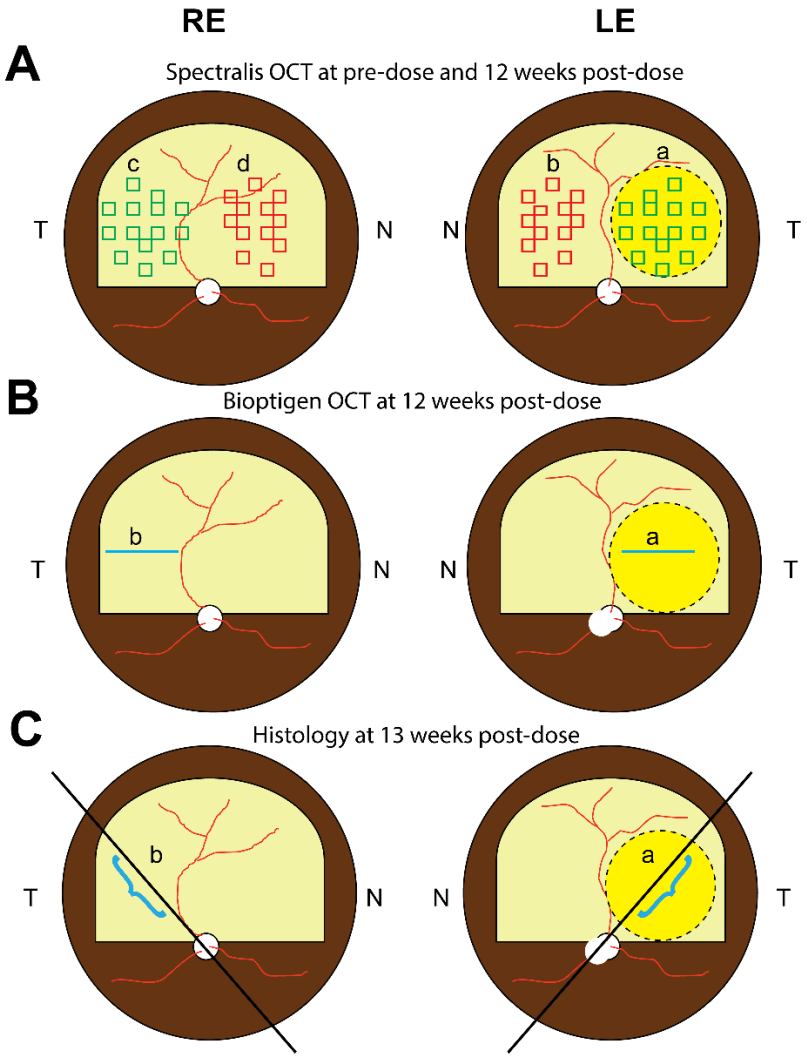

Supplementary Figure 1: Illustrations of the three different approaches used for outer nuclear layer (ONL) thickness analysis. (A) At pre-dose and 12 weeks post-dose, loci selected inside **(**green-a**)** and outside **(**red-b**)** the outermost treatment boundary of the injected left eye (LE) and their comparable areas **(**c, d**)** in the non-injected contralateral right eye (RE) were used for quantitative evaluation. **(B)** In vivo assessment at study week 12 was performed by manual segmentation of a single high-resolution (Bioptigen) OCT B-scan (a, blue line) inside the treated area of the injected eye (LE), and the comparable area (b, blue line) in the non-injected eye (RE) was used for quantification. **(C)** Quantification of ONL thickness by histology was performed on a single section (black line) that extended through the central region of the bleb/treated area and optic disk in the injected eye (LE) and a comparable area of the non-injected eye (RE). Selection of four locations within the bleb/treated area (a) and equivalent area (b) in OD are illustrated by the blue bracket. N, nasal retina; RE, right eye; LE, left eye; T, temporal.

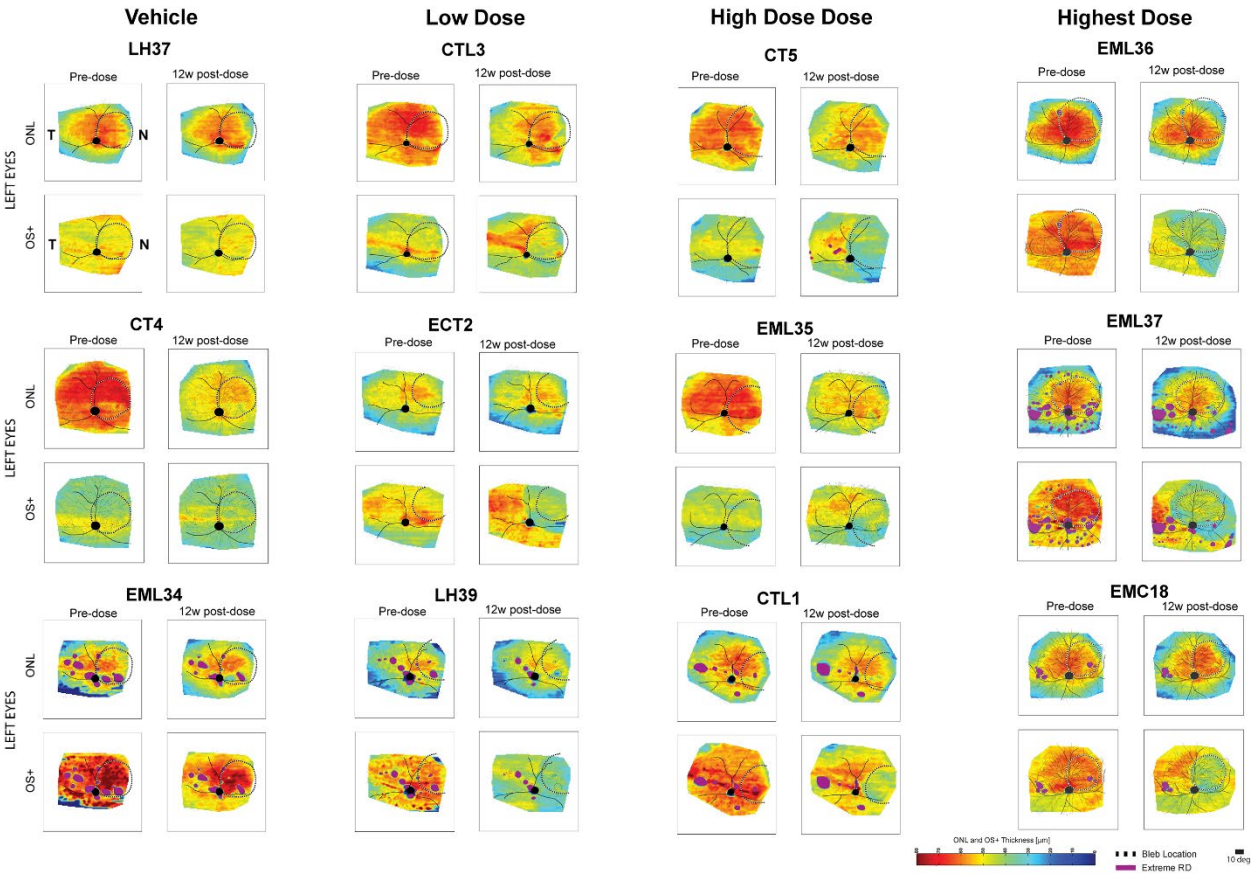

Supplementary Figure 2: **Pseudocolor maps of outer nuclear layer and RPE-Photoreceptor interface thicknesses at pre-dose and 12 weeks post-dose of all injected eyes.** Pseudocolor ONL thickness map of all left eyes from the vehicle-injected, low-dose, high-dose, and highest dose groups. Treatment boundaries are based on fundus photographs of the bleb taken at the time of the injection (dotted lines), and, if visible, demarcations apparent on infrared imaging at the time of scanning (dashed lines). Optic nerve and major blood vessels (black) are overlaid for ease of comparison. ONL, outer nuclear layer; OS+, RPE-photoreceptor distance; N, nasal retina; T, temporal; RD, retinal detachment.

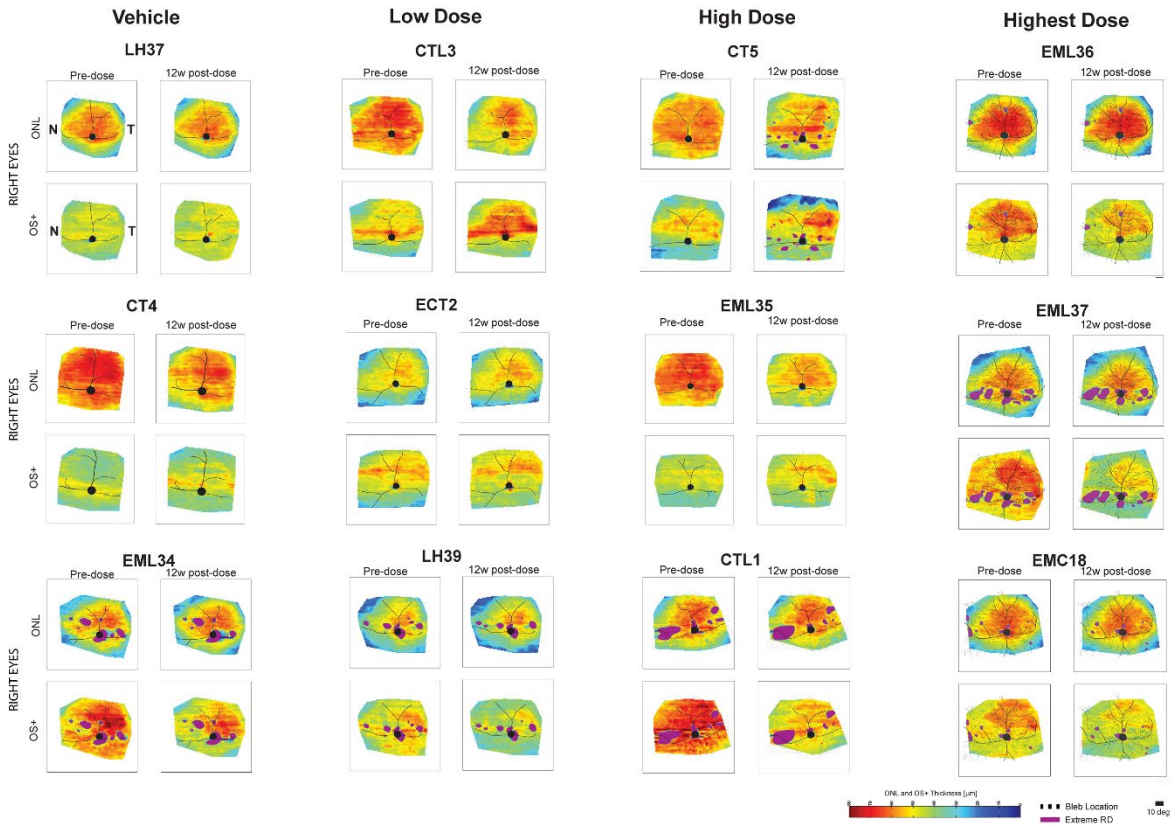

Supplementary Figure 3: **Pseudocolor maps of outer nuclear layer and RPE-Photoreceptor interface thicknesses at pre-dose and 12 weeks post-dose of all non-injected eyes.** Pseudocolor ONL thickness map of all non-injected right eyes from the vehicle-injected, low-dose, high-dose and highest-dose treatment groups (right eyes are show as left eyes). Treatment boundaries are based on fundus photographs of the bleb taken at the time of the injection (dotted lines), and, if visible, demarcations apparent on infrared imaging at the time of scanning (dashed lines). Optic nerve and major blood vessels (black) are overlaid for ease of comparison. ONL, outer nuclear layer; OS+, RPE-photoreceptor distance; N, nasal retina; T, temporal; RD, retinal detachment.

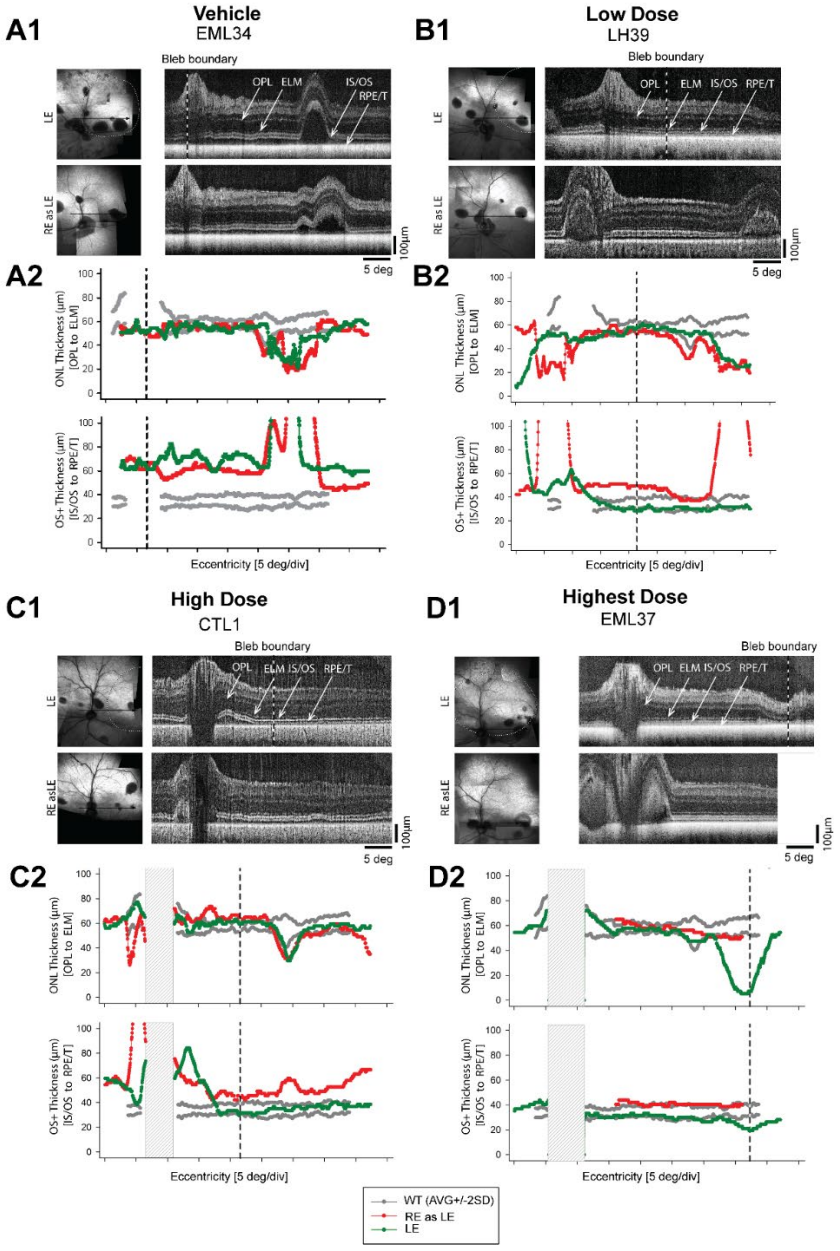

Supplementary Fig 4: **Representative high resolution optical coherence tomography (HR-OCT) images and quantification of outer nuclear layer and RPE-photoreceptor interface thicknesses at 12 weeks post-dose from all 4 treatment groups. (A1-D1)** cSLO image with black bar showing the location of the high resolution (Bioptigen) OCT b-scans in the injected left eye (LE) and same area in the non-injected right eye (RE) of one dog per treatment group. **(A2-D2)** ONL and OS+ thickness along the OCT scans shown in panels above. The dashed line represents the bleb border. The green line represents the injected LE, the red line the non-injected RE in the same area, and the grey lines demarcate the 95% confidence interval of those measurements from wild-type (WT) non-injected dogs in the same area. ONL, outer nuclear layer; OS+, RPE-photoreceptor distance; Right eyes are shown as left eyes (RE as LE).

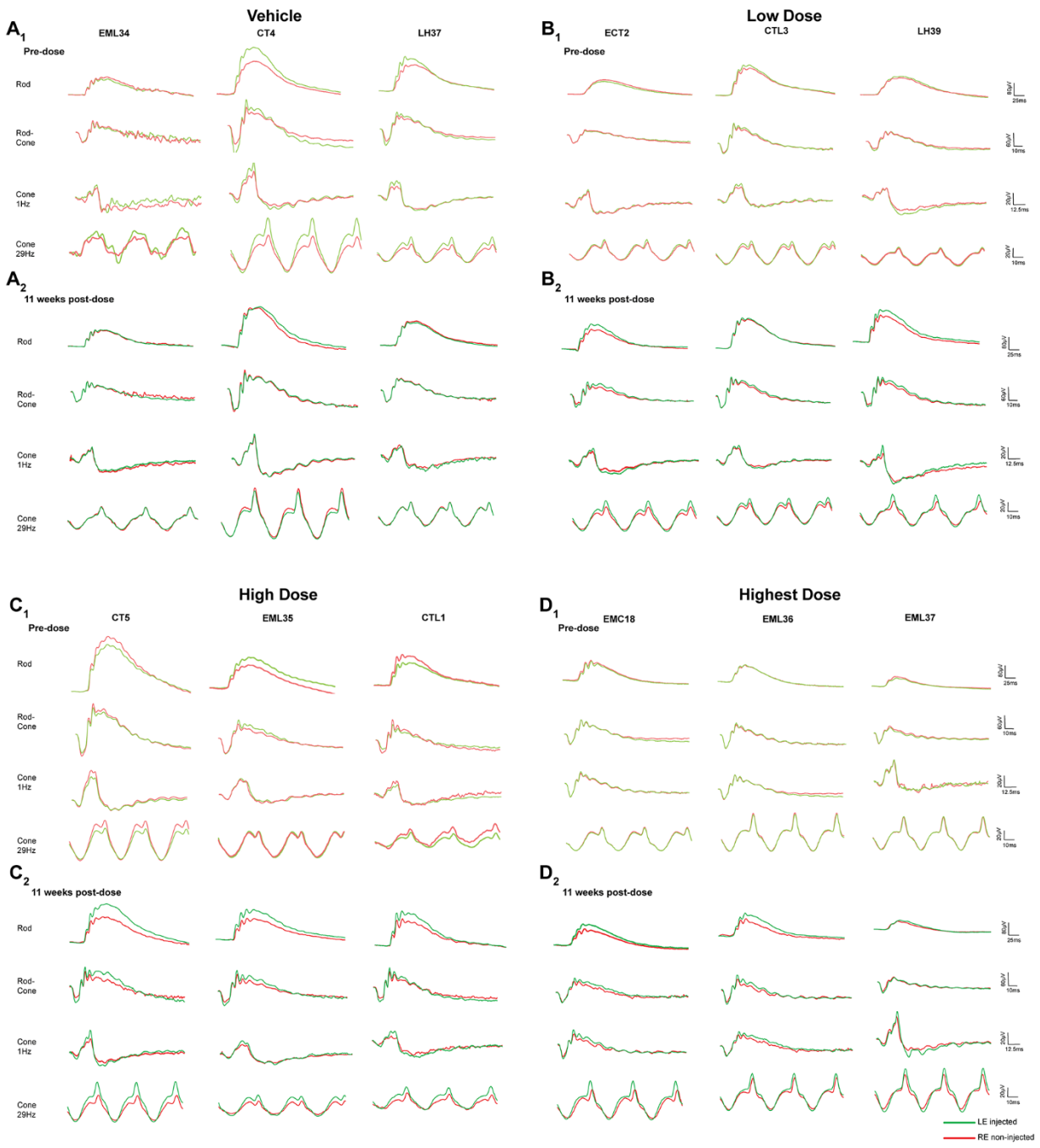

Supplementary Figure 5: **Full field electroretinographic (ERG) traces from all dogs within each treatment group.** Recordings of rod (-1.74 log cd.s.m^{-2}), mixed rod–cone (0.5 log cd.s.m^{-2}), and cone responses to 1Hz stimuli (0.5 log cd.s.m^{-2}) or 29Hz cone flicker (0.25 log cd.s.m^{-2}) at pre-dose **(A)** and 11 weeks post-dose (**B**). The green traces are from the injected left eyes (LE), and the red traces from the non-injected right eyes (RE).

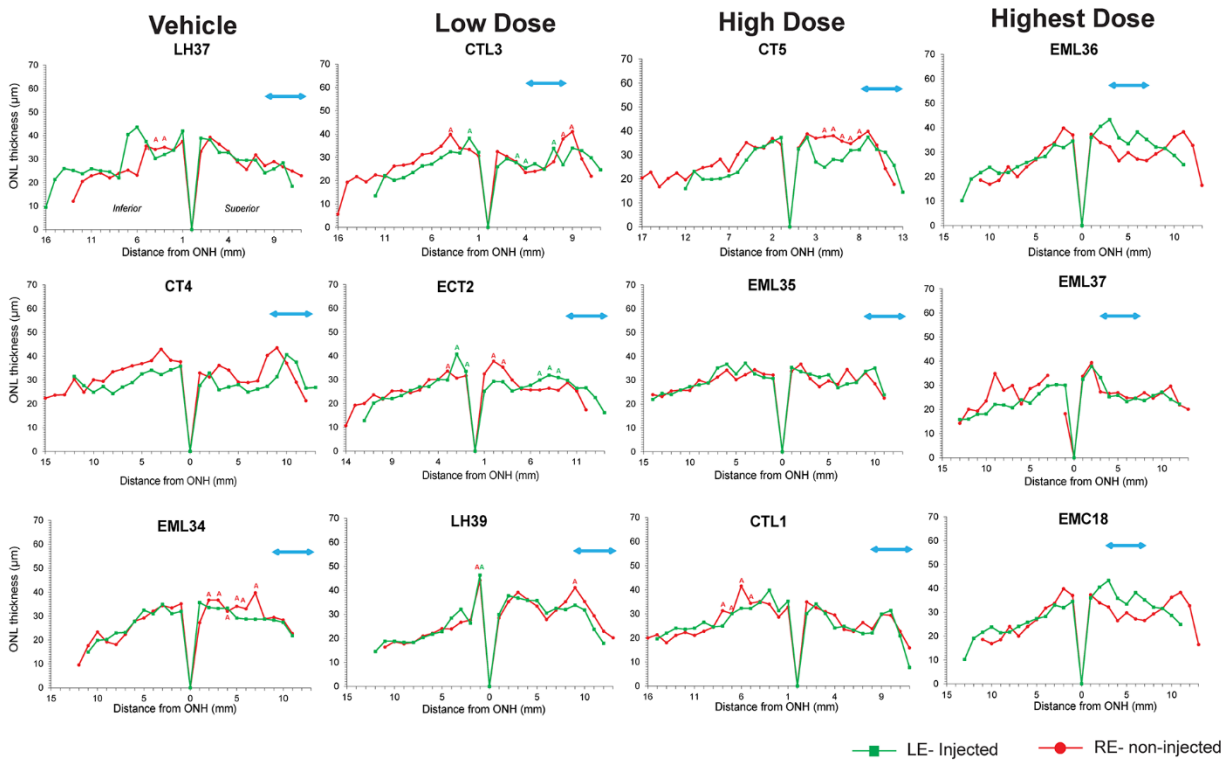

Supplementary Figure 6: Outer nuclear layer thickness quantified by histology at 13 weeks post-dose. Spidergraphs of ONL thickness from both eyes (green traces = LE/injected eyes; red traces = RE/non-injected eyes) extending from the optic nerve head (ONH) to the peripheral *ora serrata* along both the inferotemporal and supero-nasal quadrants for all the dogs in all treatment groups. Blue bar above x axis of spidergraphs corresponds to five locations within the bleb/treated area (and equivalent area in the RE) used for calculation of the mean ONL thickness. Annotations with the letter "A" indicate locations of artefactual ONL separation that occurred during histological processing. ONL, outer nuclear layer; LE, left eye; RE, right eye.

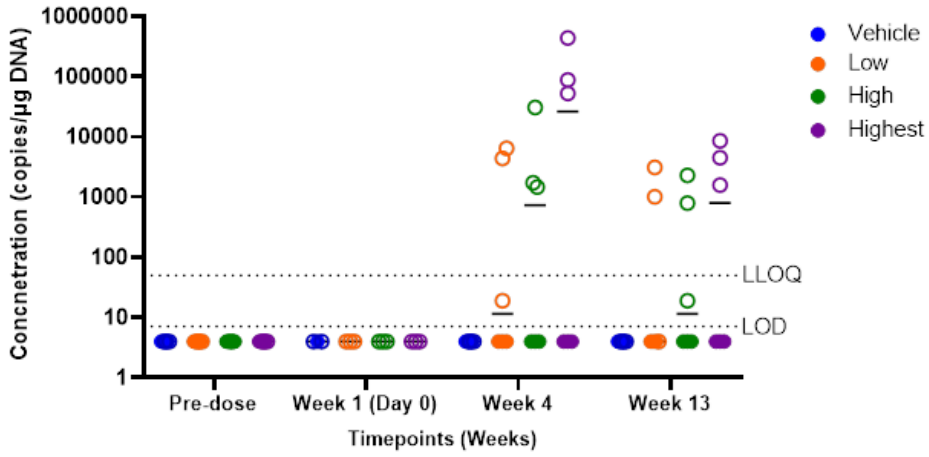

Supplementary Figure 7: Quantification of OPGx-BEST1 in the aqueous humor of both eyes following a single subretinal administration of vehicle or OPGx-BEST1 at a low, high, or highest dose in the left eye. Dashed line represents the LOD (7.14 copies/µg DNA) and LLOQ (50.00 copies/µg DNA). Negative and positive samples were attributed an arbitrary value of 4 and 19 copies/µg DNA respectively. Closed and open symbols represent data from the right and left eye respectively. Each dot represents data from one individual animal. LOD, limit of detection; LLOQ, lower limit of quantification

Supplementary Tables

Supplementary Table 1- Experimental design-summary of assessment procedures.

	Subretinal Injection	*Physical Examination + Body weight*	*Clinical Pathology*	*Biodistribution*	*Titration of AAV2 Bab*	*Aqueous Humor*	*Eye Examination, IOP, Fundus Photography*	*cSLO + SR-OCT*	*HR-OCT*	*ERG*	*Termination and Necropsy*
Pre-dose		X	X	X	X	X	X	X		X	
Day of dose	X	X				X (LE)					
Day 1				X							
Week 1		X	X	X	X		X	X			
Week 2		X									
Week 3		X									
Week 4		X	X	X	X	X	X	X			
Week 5		X									
Week 6		X									
Week 7		X									
Week 8		X	X	X	X		X	X			
Week 9		X									
Week 10		X									
Week 11		X								X	
Week 12		X	X		X		X	X	X		
Week 13		X		X	X	X					X

X indicates procedure performed; gray shading indicates procedure not performed.
cSLO + SR-OCT: confocal scanning laser ophthalmoscopy + standard resolution spectral domain optical coherence tomography; HR-OCT: high resolution spectral-domain optical coherence tomography; ERG: electroretinography; IOP: intraocular pressure; Bab, blocking antibodies.

Supplementary Table 2- Summary of ophthalmic findings in non-injected eyes.

Finding	Pre-dose	Study Week 1	Study Week 4	Study Week 8	Study Week 12
Conjunctival hyperemia:					
Mild	1/12	0/12	0/12	0/12	0/12
Moderate	1/12	0/12	0/12	0/12	0/12
Periocular erythema	1/12	0/12	0/12	0/12	0/12
Fundus Exam:					
Focal areas of pigmentation	1/12	1/12	1/12	1/12	1/12
BEST1 Stage II- Vitelliform	2/12	2/12	1/12	3/12	4/12
BEST1 Stage III-Pseudo-hypopyon	6/12	6/12	6/12	6/12	6/12

Supplementary Table 3- Summary of ophthalmic findings in vehicle-injected eyes.

Finding	Pre-dose	Study Week 1	Study Week 4	Study Week 8	Study Week 12
Conjunctival hyperemia					
Mild	0/3	2/3	1/3	0/3	0/3
Fundus Exam					
Retinotomy scar	0/3	3/3	3/3	3/3	3/3
Visible border of subretinal bleb	0/3	2/3	0/3	0/3	0/3
Within treated area					
Stage II- Vitelliform	1/3	1/3	1/3	1/3	1/3
Stage III-Pseudo-hypopyon	1/3	0/3	0/3	0/3	0/3
Other: White material in inferior bleb area	0/3	1/3	0/3	0/3	0/3
Within untreated area					
Stage II- Vitelliform	1/3	1/3	1/3	1/3	2/3
Stage III-Pseudo-hypopyon	1/3	1/3	1/3	1/3	1/3

Supplementary Table 4- Summary of ophthalmic findings in low-dose OPGx-BEST1-Injected eyes.

Finding	Pre-dose	Study Week 1	Study Week 4	Study Week 8	Study Week 12
Mild blepharospasm	0/3	1/3	0/3	0/3	0/3
Conjunctival hyperemia					
Mild	1/3	3/3	0/3	1/3	0/3
Moderate	1/3	0/3	0/3	0/3	0/3
Periocular erythema	1/3	0/3	0/3	0/3	0/3
Vitreous					
Vitreal strand/fibrin	0/3	2/3	1/3	0/3	0/3
Fundus Exam					
Retinotomy scar	0/3	1/3	1/3	1/3	2/3
Within treated area					
Stage II- Vitelliform	0/3	0/3	0/3	1/3	1/3
Stage III-Pseudo-hypopyon	1/3	1/3	1/3	0/3	0/3
Within untreated area					
Stage III-Pseudo-hypopyon	1/3	1/3	1/3	1/3	1/3
Other: retinal fold, hyperreflectivity	0/3	1/3	1/3	1/3	1/3
Other: bleb incompletely reattached	0/3	1/3	0/3	0/3	0/3

Supplementary Table 5- Summary of ophthalmic findings in high dose OPGx-BEST1-Injected eyes.

Finding	Pre-dose	Study Week 1	Study Week 4	Study Week 8	Study Week 12
Conjunctival hyperemia					
Mild	0/3	1/3	1/3	2/3	1/3
Moderate	0/3	1/3	0/3	1/3	0/3
Conjunctival chemosis					
Mild	0/3	0/3	0/3	1/3	0/3
Fundus Exam					
Retinotomy scar	0/3	3/3	3/3	3/3	3/3
Within treated area					
Stage III-Pseudo-hypopyon	1/3	0/3	0/3	0/3	0/3
Other: Retinal folds	0/3	1/3	0/3	0/3	0/3
Other: Change in reflectivity	0/3	0/3	0/3	0/3	1/3
Within untreated area					
Stage II- Vitelliform	1/3	1/3	1/3	2/3	2/3
Stage III-Pseudo-hypopyon	1/3	1/3	1/3	1/3	1/3

Supplementary Table 6- Summary of ophthalmic findings in highest dose OPGx-BEST1-Injected eyes.

Finding	Pre-dose	Study Week 1	Study Week 4	Study Week 8	Study Week 12
Conjunctival hyperemia:					
Mild	1/3	2/3	2/3	1/3	1/3
Chemosis:					
Mild	1/3				
Fundus Exam:					
Retinotomy scar	0/3	1/3	1/3	1/3	1/3
Within treated area:					
BEST1 Stage II-Vitelliform	1/3	0/3	0/3	0/3	0/3
BEST1 Stage III-Pseudo-hypopyon	2/3	1/3	1/3	1/3	0/3
Other: Retinal folds	0/3	1/3	1/3	1/3	1/3
Other: Grey coloration in bleb area	0/3	1/3	3/3	3/3	3/3
Within untreated area:					
BEST1 Stage III-Pseudo-hypopyon	1/3	1/3	1/3	1/3	1/3